NASA MEMO 12-5-58W

NASA

MEMORANDUM

INTERACTION EFFECTS PRODUCED BY JET EXHAUSTING LATERALLY NEAR BASE OF OGIVE-CYLINDER MODEL IN SUPERSONIC MAIN STREAM

By P. W. Vinson, J. L. Amick, and H. P. Liepman

University of Michigan

NATIONAL AERONAUTICS AND SPACE ADMINISTRATION

WASHINGTON

February 1959

NATIONAL AERONAUTICS AND SPACE ADMINISTRATION

MEMORANDUM 12-5-58W

INTERACTION EFFECTS PRODUCED BY JET EXHAUSTING LATERALLY NEAR BASE OF OGIVE-CYLINDER MODEL IN SUPERSONIC MAIN STREAM

By P. W. Vinson, J. L. Amick, and H. P. Liepman

SUMMARY

The experimentally determined interaction effects of a side jet exhausting near the base of an ogive-cylinder model are presented and discussed. The interaction force appears to be independent of main-stream Mach number, boundary-layer condition (laminar or turbulent), angle of attack, and forebody length. The ratio of interaction force to jet force is found to be inversely proportional to the square root of the product of jet stagnation-to-free-stream pressure ratio and jet-to-body diameter ratio.

INTRODUCTION

One attractive method of controlling the flight path or attitude of a space vehicle is by means of gas jets directed normal to the body axis. Since such side jets could also give useful control forces during atmospheric flight, the interaction of a side jet with a supersonic flow is of interest. This report presents the results of a continuing investigation of these interaction effects.

Reference 1 and an unpublished report contain results of investigations of the interaction effects of a side jet issuing near the center of gravity of a cone-cylinder model. The results of these investigations indicated that the interaction effects were negligible but it was noted that the interaction effects need not be small for other jet locations. The present investigation was undertaken to determine the magnitude of the interaction effects of a side jet issuing near the base of an ogive-cylinder model.

Data on the interaction force were obtained by measuring, with a sting balance, the normal forces due to a side jet discharging into a supersonic main stream and into a vacuum. Comparison of these two cases gave the interaction force. Interaction forces were measured for

laminar and turbulent boundary layers, model forebody lengths of 3.4 and 5.4 body diameters, angles of attack from -12° to 14°, various afterbody lengths from 0.0625 to 0.625 body diameters, main-stream Mach numbers of 2.84 and 3.90, circular jet orifices of 0.159- and 0.221-inch diameter, and jet stagnation-to-free-stream static-pressure ratios of 10 to 900. Schlieren photographs of representative runs were obtained to aid in a qualitative analysis of the interaction effects. Base-pressure measurements were made to determine the effect of the side jet on model drag for both laminar and turbulent boundary layers.

This work was conducted at the Department of Aeronautical Engineering, University of Michigan, under the sponsorship and with the financial assistance of the National Advisory Committee for Aeronautics.

SYMBOLS

A_j	cross-sectional area of jet orifice
A_m	cross-sectional area of model
D	diameter of model
d	diameter of jet orifice
L	distance from model nose to center of jet orifice
l	distance from center of jet orifice to model base
M	Mach number
N	normal force
N_Δ	normal-force increment due to jet (normal force on model in main stream with jet on minus normal force due to main stream alone at same angle of attack)
N_I	interaction force, $N_\Delta - N_V$
N_V	normal force due to jet exhausting into vacuum
N_{V_t}	theoretical value of N_V, $2\left(\frac{2}{\gamma + 1}\right)^{\frac{1}{\gamma-1}} p_{o_j} A_j$
p	pressure

p_a	ambient pressure
X	location of line of action of normal force from center of jet orifice
α	angle of attack
γ	ratio of specific heats of jet gas
δ	angle through which main stream ahead of side jet is turned

Subscripts:

o	stagnation conditions
1	free-stream conditions
b	model-base conditions
j	jet conditions
t	theoretical

THEORETICAL METHODS

In attempting to provide a theoretical basis for the observed interaction effects, an analysis of a two-dimensional isentropic jet expansion has been made. The jet is assumed to expand isentropically, separating the boundary layer and causing the main flow to turn through an angle δ upstream of the jet as shown in the sketch below.

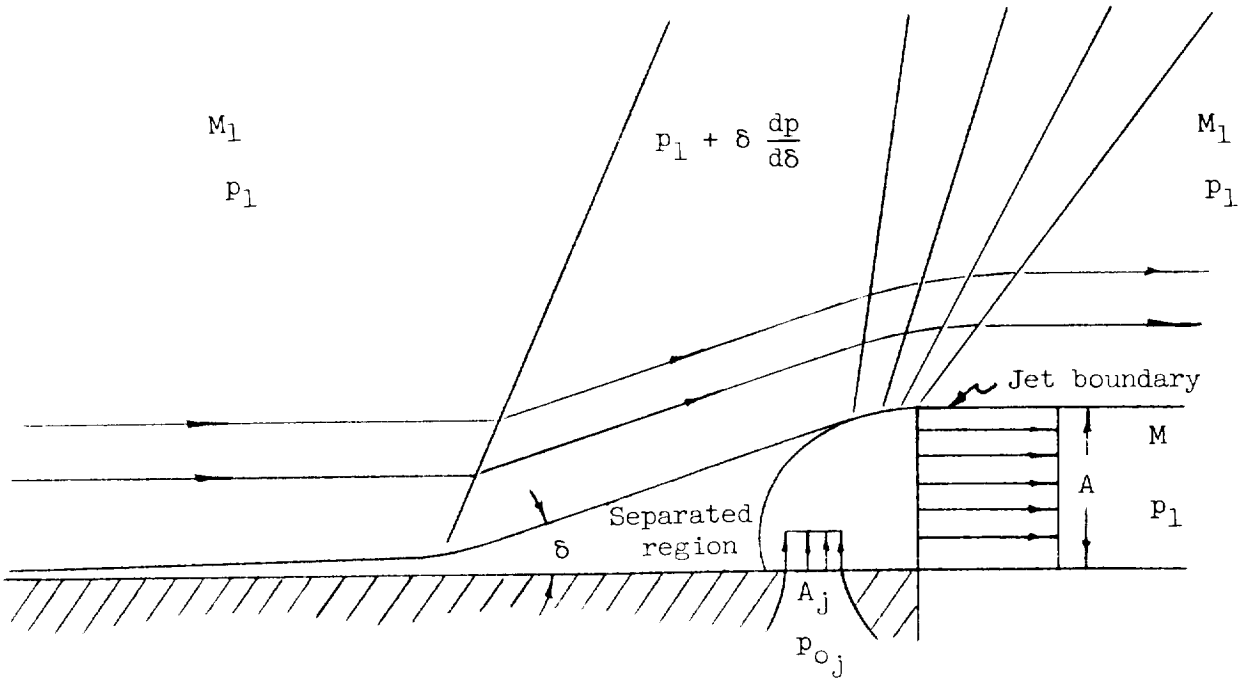

This angle δ will be small if the separated boundary layer remains laminar and somewhat larger if the separated layer becomes transitional or turbulent. The boundary-layer thickness is neglected, so that the only influence of the boundary layer is this effect on the angle δ.

Assuming that no diffusion occurs across the jet boundary and that sonic conditions exist at the throat of the jet orifice, conservation of jet mass flow requires that

$$\frac{A}{A_j} = \left(\frac{2}{\gamma + 1}\right)^{\frac{\gamma+1}{2(\gamma-1)}} \frac{\left(1 + \frac{\gamma - 1}{2} M^2\right)^{\frac{\gamma+1}{2(\gamma-1)}}}{M}$$

Mach number is related to the ratio of total to static pressure by the equation

$$\frac{p_{o_j}}{p_1} = \left(1 + \frac{\gamma - 1}{2} M^2\right)^{\frac{\gamma}{\gamma-1}}$$

Combining these two equations provides an expression for the area ratio A/A_j in terms of the pressure ratio p_{o_j}/p_1

$$\frac{A}{A_j} = \left(\frac{2}{\gamma + 1}\right)^{\frac{\gamma+1}{2(\gamma-1)}} \frac{\left(\frac{p_{o_j}}{p_1}\right)^{\frac{\gamma+1}{2\gamma}}}{\sqrt{\frac{2}{\gamma - 1}\left[\left(\frac{p_{o_j}}{p_1}\right)^{\frac{\gamma-1}{\gamma}} - 1\right]}}$$

The theoretical interaction force is equal to the unbalanced pressure in the separated region times the area exposed to separation:

$$N_{I_t} = \left(p_1 + \delta \frac{dp}{d\delta} - p_1\right) \frac{A}{\tan \delta}$$

For small angles the tangent approximates the angle and

$$N_{I_t} = A \frac{dp}{d\delta}$$

The ratio of theoretical interaction force to theoretical jet force is

$$\frac{N_{I_t}}{N_{V_t}} = \frac{A \frac{dp}{d\delta}}{2\left(\frac{2}{\gamma + 1}\right)^{\frac{1}{\gamma-1}} p_{o_j} A_j}$$

Substitution for the area ratio yields an expression for N_{I_t}/N_{V_t} in terms of p_{o_j}/p_1

$$\frac{N_{I_t}}{N_{V_t}} = \frac{1}{2}\left(\frac{2}{\gamma + 1}\right)^{1/2} \frac{\frac{d(p/p_1)}{d\delta}}{\left(\frac{p_{o_j}}{p_1}\right)^{\frac{\gamma-1}{2\gamma}} \left\{\frac{2}{\gamma - 1}\left[\left(\frac{p_{o_j}}{p_1}\right)^{\frac{\gamma-1}{\gamma}} - 1\right]\right\}^{1/2}}$$

The two-dimensional theory then indicates that pressure ratio p_{o_j}/p_1, jet-gas specific-heat ratio γ, and rate of change of static-pressure with flow deflection angle $d(p/p_1)/d\delta$ are the important parameters controlling the interaction effects. Since $d(p/p_1)/d\delta$ increases slightly with Mach number, the interaction effects should increase with Mach number. Note that the separation angle δ does not appear in the final equation, so that the interaction force is predicted by this simple analysis to be independent of the state of the boundary layer.

Figure 1 is a plot of the two-dimensional theory and shows the predicted interaction force for an air jet ($\gamma = 1.4$), exhaust gases ($\gamma = 1.2$), and monatomic gases ($\gamma = 1.67$).

It should be noted that in the above analysis a term $p_1 A_j$ has been neglected for reasons of simplicity. This term is the resultant of the pressure force acting on the inside of the body when the jet is off. The difference in normal force N_Δ between jet-on and jet-off conditions can be divided into an increment in normal force $(N_\Delta)_{outside}$ due to the jet-on—jet-off pressure differences on the outside of the body plus an increment $(N_\Delta)_{inside}$ due to the jet-on—jet-off pressure

differences on the inside of the body. Thus

$$N_I = (N_\Delta)_{outside} + (N_\Delta)_{inside} - N_V$$

$$= (N_\Delta)_{outside} + N_V - p_1 A_j - N_V$$

$$= (N_\Delta)_{outside} - p_1 A_j$$

Therefore, to be strictly correct, the equation derived above for N_{I_t}/N_{V_t} should be modified by subtracting from the right-hand side the term

$$\frac{1}{2\left(\frac{2}{\gamma + 1}\right)^{\frac{1}{\gamma-1}} \frac{p_{o_j}}{p_1}}$$

which equals $p_1 A_j / N_{V_t}$.

EXPERIMENTAL TECHNIQUES

Apparatus

The present data were obtained in the University of Michigan 8- by 13-inch Supersonic Wind Tunnel utilizing the Mach 2.84 and Mach 3.90 nozzle blocks. This tunnel is of the intermittent blowdown-from-atmospheric-pressure type with run times up to 20 seconds. The Reynolds number at Mach 2.84 is about 0.20×10^6 per inch and at Mach 3.90 is about 0.13×10^6 per inch. Calibration of the flow produced by the Mach 2.84 and Mach 3.90 nozzle blocks is reported in references 2 and 3.

Jet air pressures above atmospheric were obtained from the shop air line at a pressure of approximately 90 psig. Two Grove regulators were installed parallel in the jet air line to provide pressure regulation, and a manually operated plug valve downstream of the regulators provided on-off control of air flow to the model.

Jet air pressures less than atmospheric were obtained by breaking the air supply line upstream of the plug valve. Atmospheric air was then throttled to the desired pressure by partially closing the plug valve.

The shop air was contaminated with a certain amount of entrained . The effect of oil contamination was considered negligible since ere were no discernible differences between the atmospheric and shop air data. The only apparent effect was to cause oil streaks on the tunnel window toward which the jet was directed for some of the schlieren photographs.

Normal-force data were obtained from two 4-element strain-gage bridges mounted on flats milled in a hollow steel sting which also served as the supply line for jet air. A multichannel, bridge-type amplifier provided strain-gage excitation and amplified the output signal sufficiently to drive a sensitive oscillograph galvanometer. Test data were recorded on photographic paper for subsequent reduction. Calibration data were obtained after each series of runs by hanging weights on the end of the sting and recording galvanometer deflections.

A Pitot tube and thermocouple were located inside the sting near the jet orifice providing jet stagnation-pressure and temperature data. The thermocouple output was sufficient to drive a galvanometer without intermediate amplification. Jet stagnation pressures greater than atmospheric were read directly on a pressure gage while subatmospheric pressures were read on a mercury manometer.

Models

The models tested consisted of various combinations of the components shown in figure 2. The base, containing the jet orifice, had internal threads for attachment to the hollow sting and an "O" ring seal to prevent jet air leakage. The two forebodies shown were attached to the front of the base also by means of threads and an "O" ring seal. The spacers were attached to the base in various combinations to give the desired afterbody lengths.

Each of the two forebodies had an ogive-shaped nose 3 diameters long followed by a 2-inch-diameter cylinder. When mounted on the base they gave nose-to-orifice distances L of 3.4 and 5.4 diameters.

Two different jet orifice diameters were tested. After tests had been made on the smaller diameter orifice, d = 0.159 inch, the orifice was plugged and a larger orifice, 0.221 inch in diameter, was drilled in the opposite side of the base. Views of the assembled model showing the two orifice sizes appear in figure 3. The short forebody (L/D = 3.4) is shown attached to the base with the complete set of afterbody spacers. The ring shown on the nose of the model was used to provide a turbulent boundary layer for some of the tests.

Details of the internal orifice geometry are shown in the sketch below

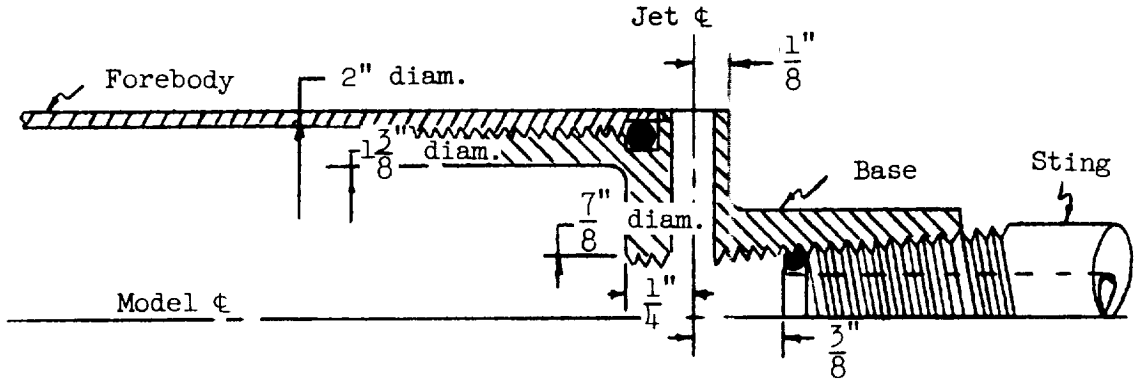

Both orifices tested entered the base in the portion threaded for sting attachment. The actual orifice entry details then varied somewhat for the two orifices tested.

The complete model sting assembly is shown in figure 4.

Tests

Jet tare-force calibrations were obtained by evacuating the test section to approximately 2 inches of mercury absolute pressure and shielding the model externally from the jet blast. The purpose of the shielding was to produce a more nearly uniform pressure on the outside of the model. The force measured was equal to N_V minus a small term $p_a A_j$ which was due to the ambient pressure p_a surrounding the model. Although the pressure p_a was not measured, it was believed to be somewhat less than the pressure outside the shield and of the same order as the free-stream pressure p_1 at the Mach number 2.84.

In the data reduction no correction was made for $p_a A_j$, and the measured force was used directly as N_V. Figure 5 shows the variation of N_V/N_{V_t} (where N_V is the measured jet force uncorrected for $p_a A_j$) with p_{o_j} for the two orifices tested. These curves were used to obtain the interaction force from the measured net normal force N_Δ and the theoretical jet force N_{V_t} according to the equation

$$\frac{N_I}{N_V} = \frac{N_\Delta}{N_{V_t}\left(\frac{N_V}{N_{V_t}}\right)} - 1$$

The data reduced in this manner are approximately comparable to the values of N_{I_t}/N_{V_t} given by the simple two-dimensional theory in which the term $p_1 A_j$ is neglected.

Tests were made at Mach 2.84 with the long forebody (L/D = 5.4) and a laminar boundary layer, but china-clay patterns of the boundary-layer separation were irregular and unsymmetrical, indicating an unstable laminar boundary layer. This boundary-layer instability was attributed to interaction of tunnel disturbances with the model, and subsequent runs were made with the boundary-layer trip on the model nose. Data on the variation of the interaction force with jet stagnation pressure, angle of attack, and afterbody length were obtained for the long-forebody, turbulent-boundary-layer model.

China-clay patterns of the boundary-layer separation at Mach 2.84 on the short forebody (L/D = 3.4) indicated a stable laminar boundary layer, and data were obtained for both laminar and turbulent boundary layers. In addition, data were obtained for the two orifice diameters and for various afterbody lengths.

At Mach 3.9 it was found that a stable laminar boundary layer existed on both the short and long models. Consequently, data were obtained for both models with laminar and turbulent boundary layers. Unfortunately, an amplifier maladjustment rendered the bulk of the Mach 3.9 data invalid. It is felt that for the most part the long-forebody, turbulent-boundary-layer data are valid, but caution should be used in applying them.

During the initial test phase base-pressure readings were obtained by measuring the pressure inside the windshield. However, since the windshield was found to change the nature of the jet effect on base pressure, the remainder of the testing was done without base-pressure measurements except for one series of runs with the windshield removed. No attempt was made to obtain normal-force data for the "windshield-removed" runs.

Accuracy

An analysis of the probable errors in measuring normal-force magnitudes predicts a maximum probable error of ±15 percent of N_I/N_V.

The bulk of the experimental data falls within this predicted range of accuracy.

RESULTS AND DISCUSSION

Normal-Force Data

Data on the normal force due to jet interaction N_I are presented in figures 6 through 14, which cover the parameters varied in this investigation. Reference 1 contains a dimensional analysis of the parameters involved in the interaction of the jet stream with the main flow which indicates that p_{o_j}/p_1, d/D, and A_j/A_m, among others, may be important dimensionless quantities governing the interaction effects. The two-dimensional theoretical approach presented in this report indicates that only p_{o_j}/p_1 should be important for correlation of N_I/N_V data. It is natural to expect that a ratio of characteristic jet dimension to body dimension should be important in three-dimensional flow. Verification of the importance of the parameter $p_{o_j}d/p_1D$ is shown in figure 8. Good correlation of N_I/N_V data is obtained for the two jet orifice diameters tested using the dimensionless parameter $p_{o_j}d/p_1D$.

Within the limits of accuracy of the present data, main-stream Mach number, boundary-layer condition (laminar or turbulent), and L/D ratio are found to have a negligible effect upon the interaction force. While most of the angle-of-attack data fall within the predicted accuracy range, there is a definite trend of increased interaction force at negative angles of attack, and reduced interaction force at positive angles. An empirical equation

$$\frac{N_I}{N_V} = \frac{0.92}{\left(\frac{p_{o_j}d}{p_1D}\right)^{1/2}}$$

fits the experimental curve of figure 6, which contains all of the experimental data with minimum afterbody length ($l/D = 0.0625$).

Figure 13 contains data for various ratios of afterbody length to body diameter l/D from 0.0625 to 0.625. While the data again do not greatly exceed the predicted range of accuracy, there is a consistent reduction in interaction force with increasing afterbody length

Since the two-dimensional theory does not depend upon the ratio of jet orifice to body diameter, as does the experimental data, a direct comparison cannot be made. Figure 7 shows the two-dimensional theory plotted with the data for the two orifice diameters tested. Obviously the agreement of experiment with theory is dependent upon the diameter ratio and Mach number selected. However, it is important to note that the two-dimensional theory does correctly predict the reduction in interaction force with increasing pressure ratio.

Resultant normal-force location data are shown in figure 14. These data cannot be correlated, but the location of the normal force, on an average, does not exceed 0.05 body diameters from the center of the jet orifice. Thus, for all practical purposes, the normal force can be assumed to act at the center of the jet orifice.

Base-Pressure Data

Figure 15 shows the result of a circumferential base-pressure survey with the windshield removed. No attempt was made to measure radial pressure variations. The circumferential survey indicates existence of a low-pressure region directly behind the jet and a high-pressure region in the wake opposite the jet orifice. An integrated average-pressure reading occurs at a point 90° from the jet orifice. The windshield-removed data of figure 16 were obtained at the 90° location. The effect of the windshield on base pressure is apparent. No attempt was made to evaluate the effect of the presence of the sting on base pressure, although this effect is probably considerable since the sting diameter is approximately one-half that of the model. Base pressure decreases with the windshield removed and the jet on, indicating a rise in model drag due to the jet. As might be expected this decrease in base pressure due to the jet is slightly greater for a laminar boundary layer than for a turbulent boundary layer.

Schlieren Photographs and China-Clay Patterns

The schlieren photographs in figures 17 through 20 give a qualitative picture of the effect of the different parameters on interaction force. They, together with the china-clay patterns of figure 21, provide a possible explanation for the negligible effect of boundary-layer condition on interaction force. The laminar boundary-layer separation covers a larger area of the model than does the turbulent separation, but the pressure rise at separation is greater for a turbulent boundary layer than for a laminar boundary layer. These two effects are in opposition and probably explain the negligible effect of boundary-layer condition on interaction force. This experimental result is in agreement with the two-dimensional isentropic theory presented earlier, which

says that the interaction force is independent of the flow deflection angle at separation.

Combination of the spreading effect of the jet region-of-influence and the low-pressure region directly behind the jet probably accounts for the reduced interaction force with increasing afterbody length.

Jet Efficiency

Since the interaction force N_I becomes an increasingly smaller percentage of the jet force N_V as the pressure-diameter ratio parameter $p_{o_j}d/p_1D$ is increased, it is desirable to design for small values of this parameter in order to obtain a given total normal force N_Δ (i.e., $N_\Delta = N_I + N_V$) with the least jet force. This can be accomplished by using a large value of d/D and a small value of p_{o_j}/p_1. The advantage of a larger jet diameter is shown in figure 22 where normal force is plotted as a function of the jet thrust in a vacuum N_V. It is apparent that the larger jet would require somewhat less jet force to produce a given total normal force.

The jet should be located near the base to minimize the loss in interaction force due to spreading of the jet region of influence. This is particularly desirable for a laminar boundary layer where the jet spreading action is more pronounced. Having the jet near the base also reduces the body area exposed to corrosive exhaust gases should they be used as the jet medium.

RESULTS AND RECOMMENDATIONS

The interaction force produced by a jet exhausting laterally near the base of an ogive-cylinder model for the present investigation is found to be favorable and appears to be independent of main-stream Mach number, boundary-layer condition, and forebody length. Angle of attack has only a secondary effect. For an air jet located close to the base, the ratio of interaction force N_I to jet thrust N_V is $\frac{N_I}{N_V} = \frac{0.92}{\sqrt{p_{o_j}d/p_1D}}$ where $p_{o_j}d/p_1D$ is pressure-diameter ratio parameter. Increasing the body length behind the jet decreases the interaction force somewhat. A small direct drag is associated with the side jet in the form of a decrease in base pressure.

It is recommended that further investigations be made to determine, in detail, the flow field in the vicinity of a side jet. Pressure measurements over the body in the vicinity of the side jet should provide a basis for understanding the mechanism of jet and main-stream interaction. The predicted effect of utilizing exhaust gases should also be verified experimentally.

University of Michigan,
Ann Arbor, Mich., July 25, 1957.

REFERENCES

1. Morkovin, M. V., Pierce, C. A., Jr., and Craven, C. E.: Interaction of a Side-Jet With a Supersonic Main Stream. Eng. Res. Bull. No. 35, Univ. of Mich., Sept. 1952.

2. Culbertson, P. E.: Calibration Report on the University of Michigan Supersonic Wind Tunnel. Part III - Aerodynamic Calibration at Nominal Mach Number of 2.84. Part IV - Aerodynamic Calibration at Nominal Mach Number of 1.44. WTM-213, Univ. of Mich., 1952.

3. Murphy, J. C., and Sivier, K. R.: Progress Report on Mach 4 Nozzle Calibration. WTM-199, Univ. of Mich., 1951.

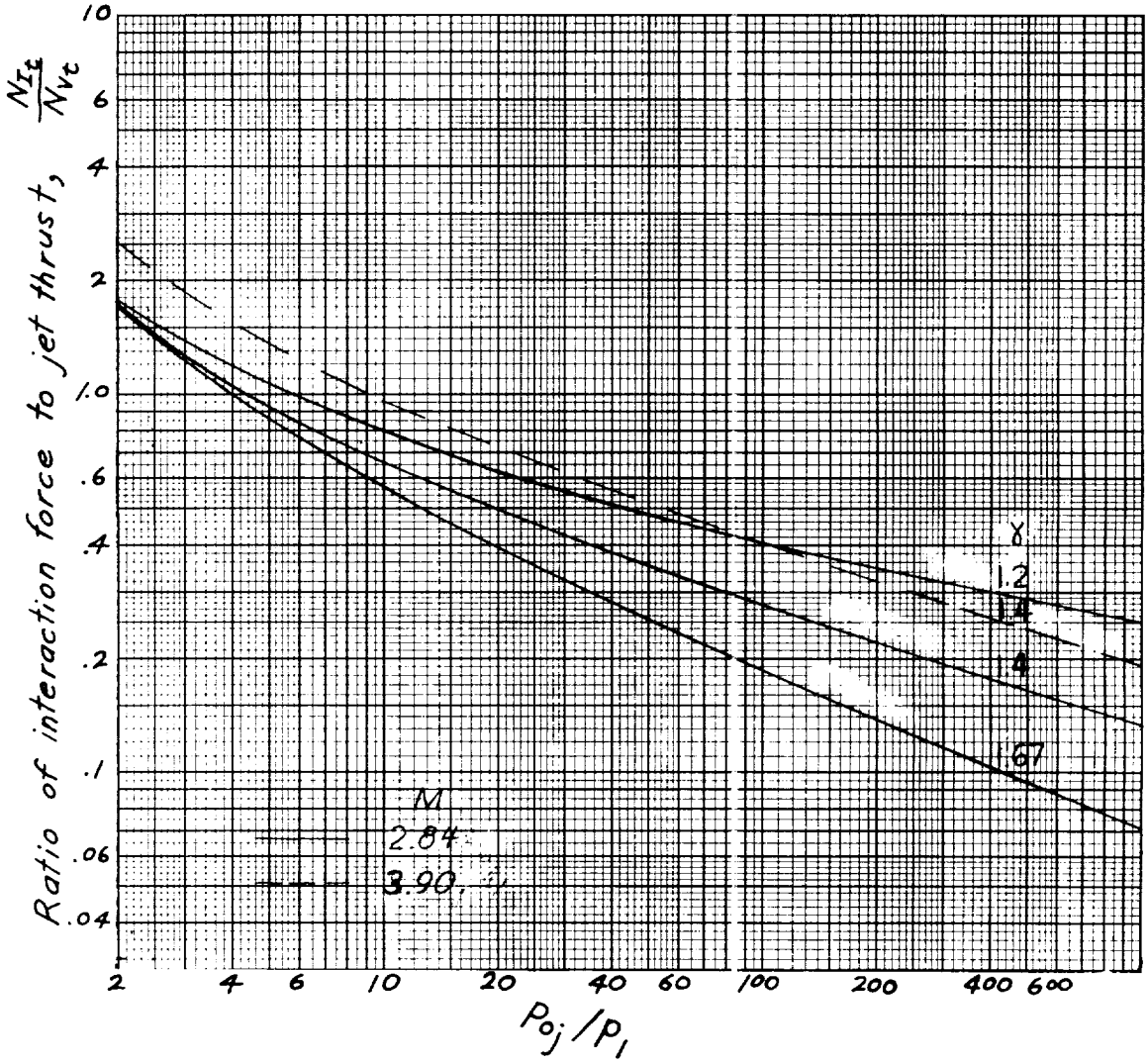

Figure 1.- Two-dimensional isentropic theory.

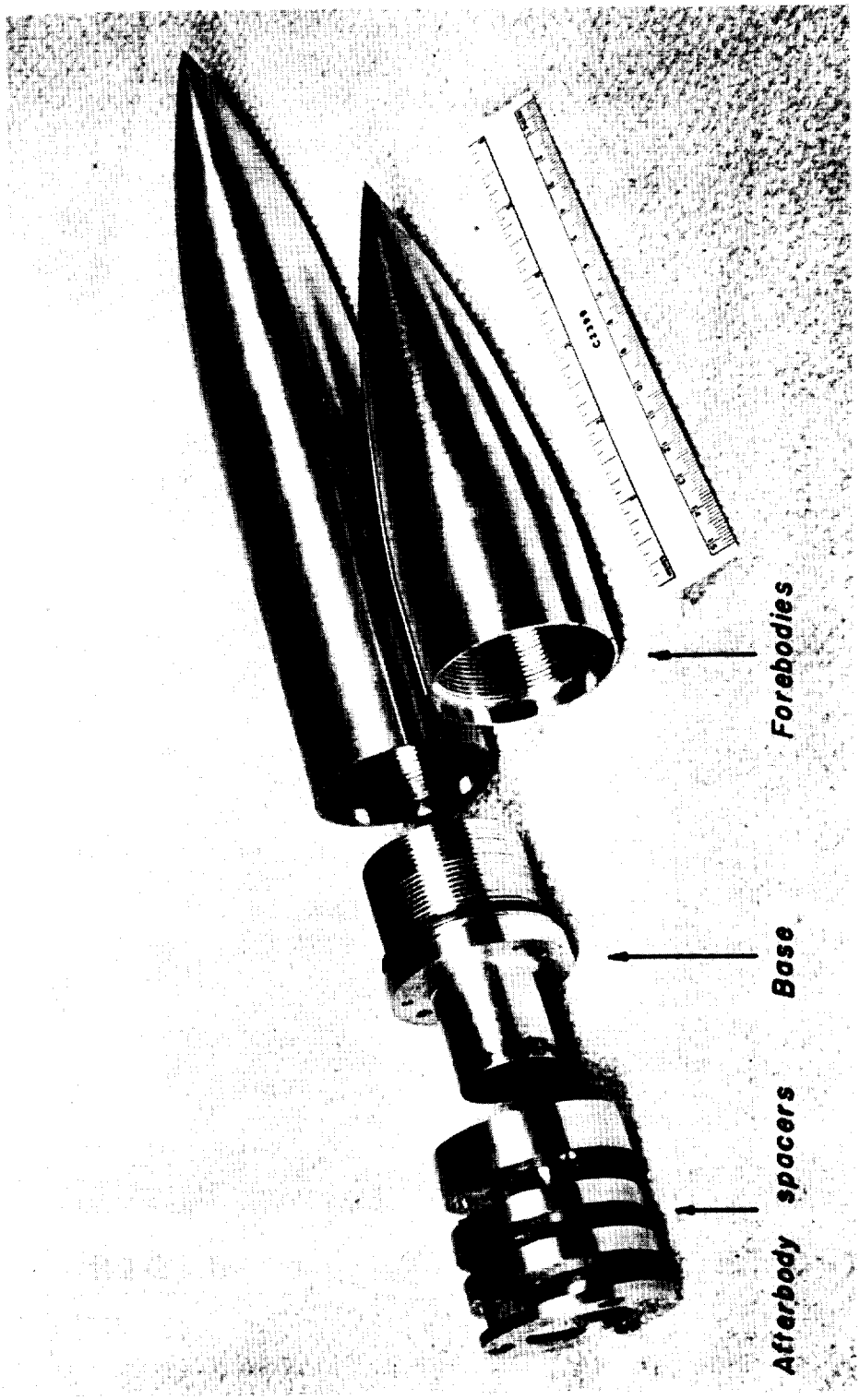

L-58-3962

Figure 2.- Exploded view of side jet model.

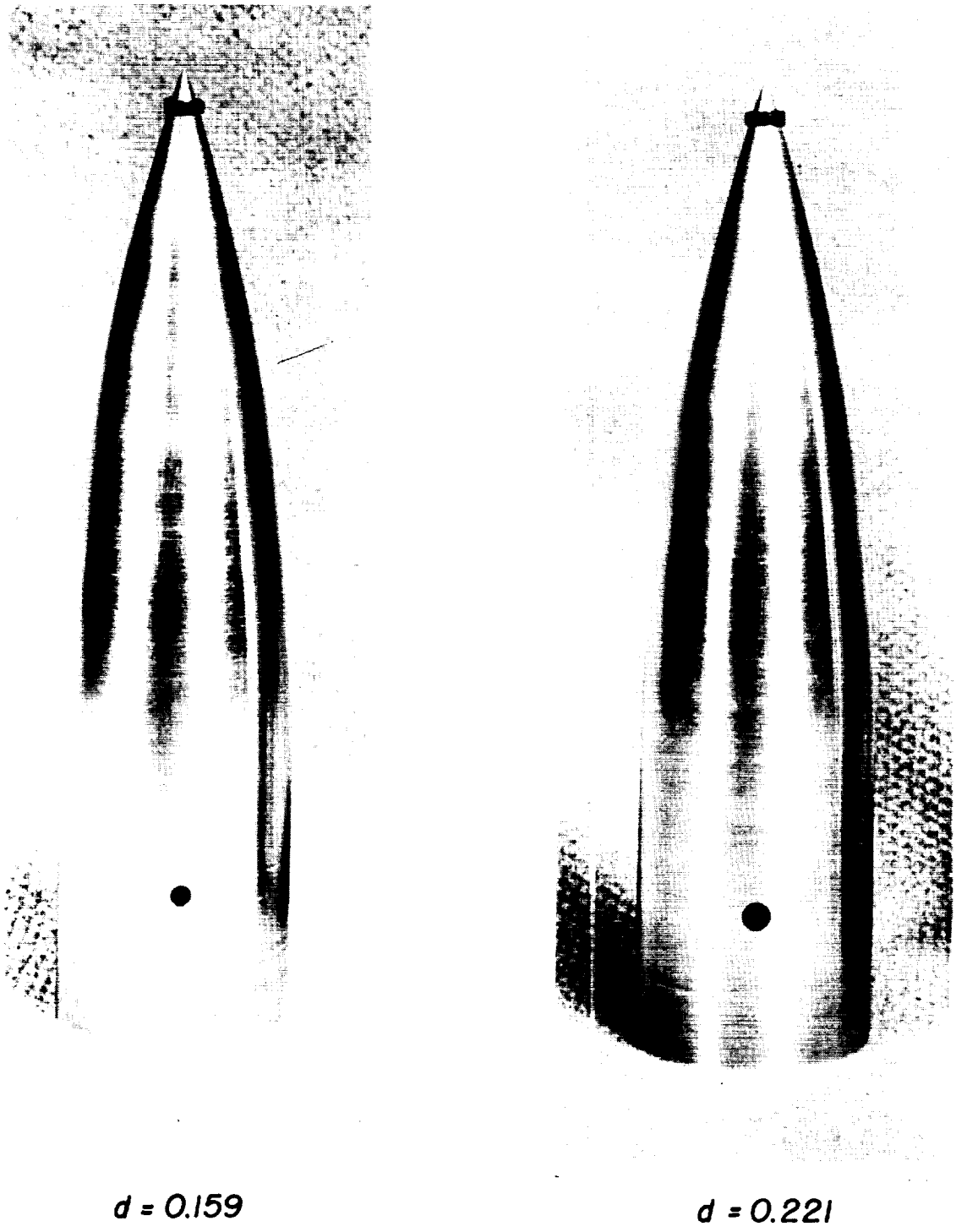

L-58-3963

Figure 3.- Side jet model (L/D = 3.4), afterbody spacers and boundary-layer trip attached.

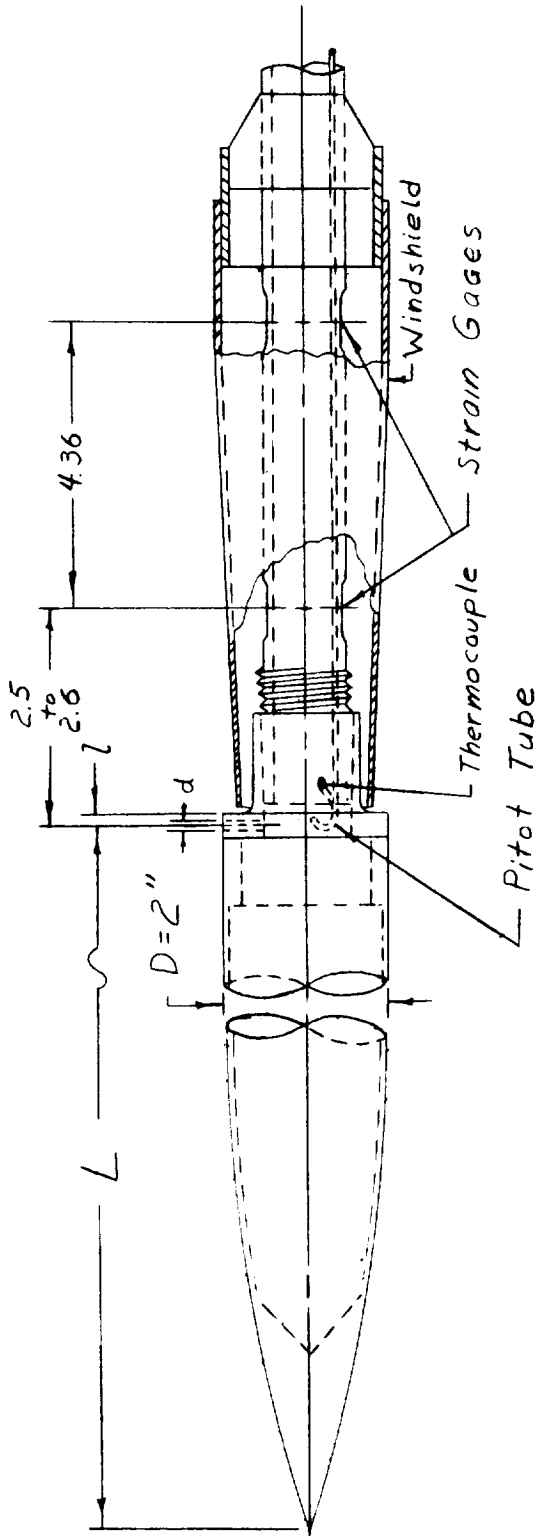

Figure 4.- Model sting assembly.

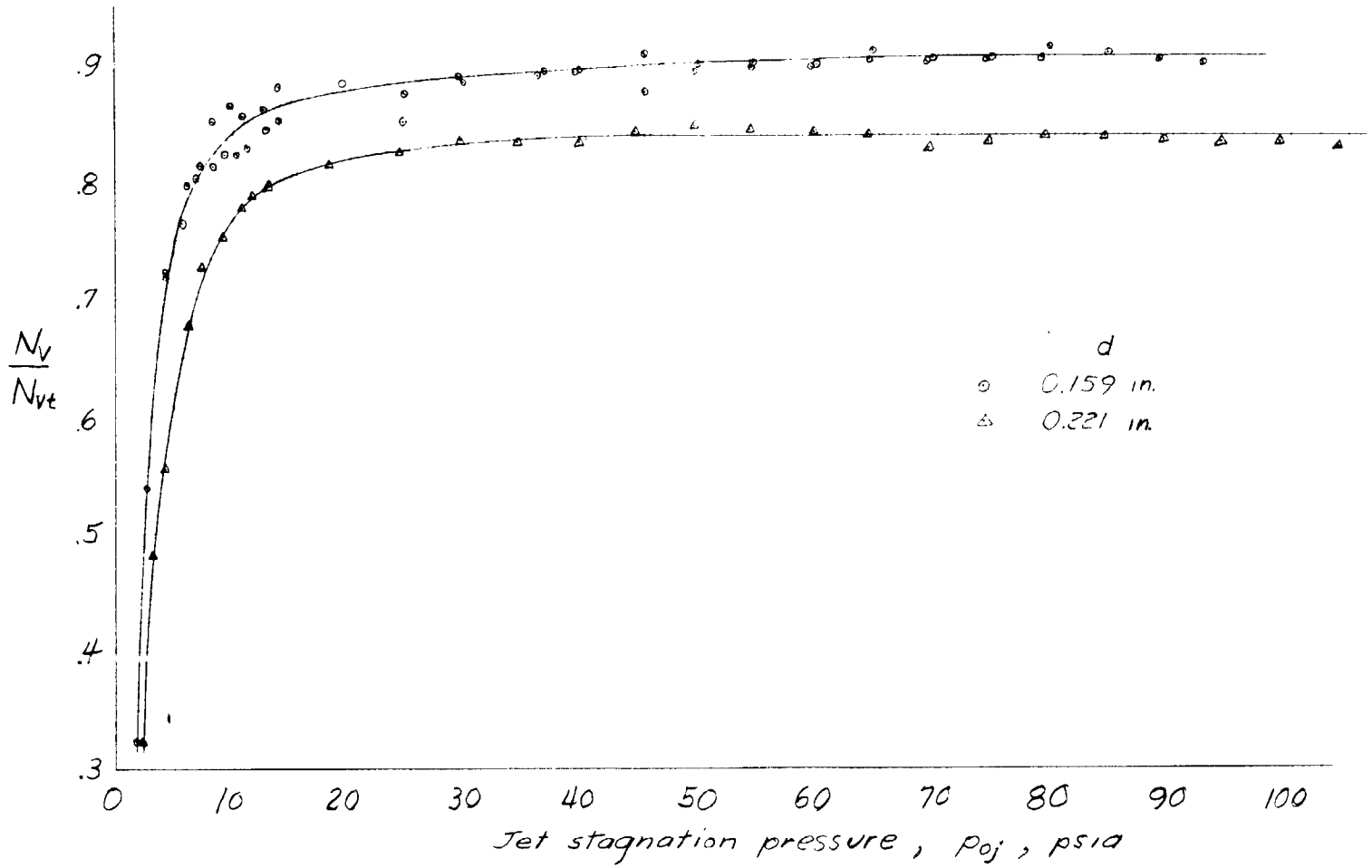

Figure 5.- Jet-tare-force calibration. Jet exhausting into a vacuum; model shielded externally.

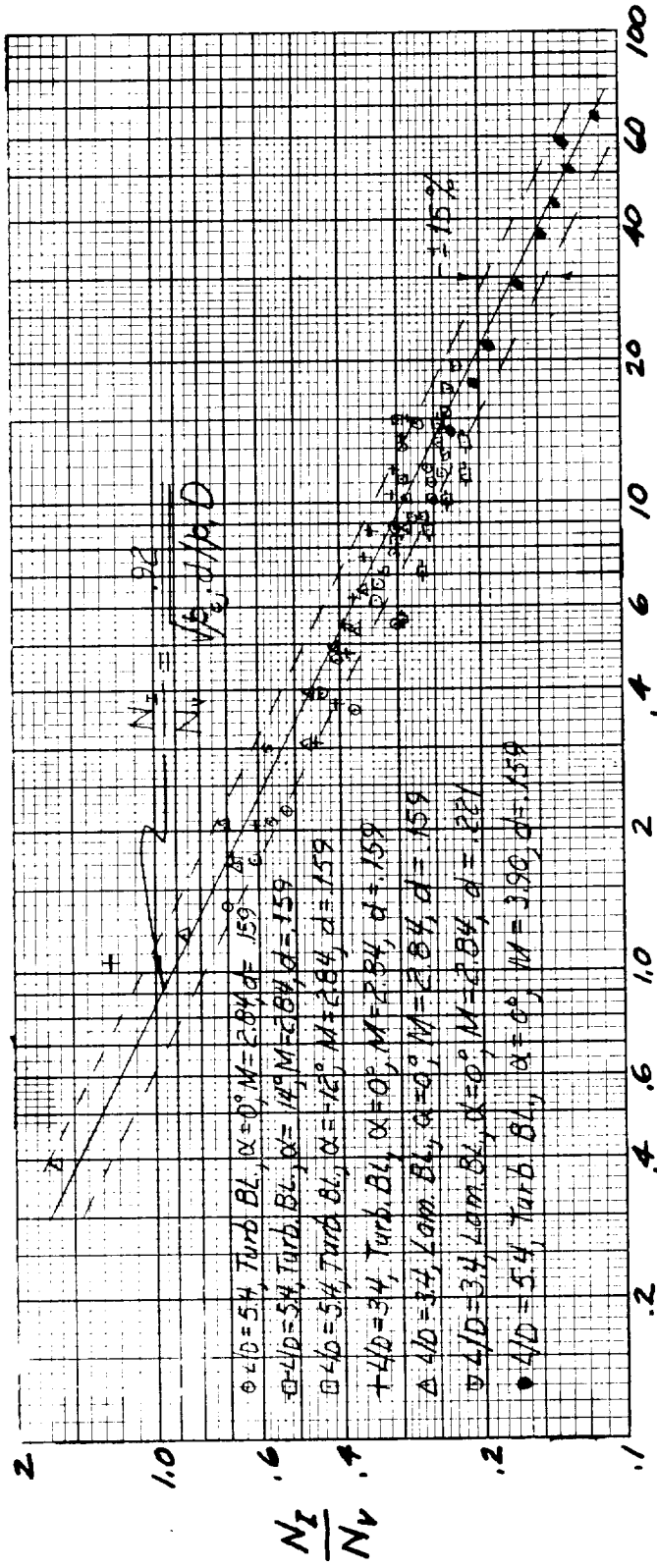

Figure 6.- Correlation of experimental data, l/D = 0.0625.

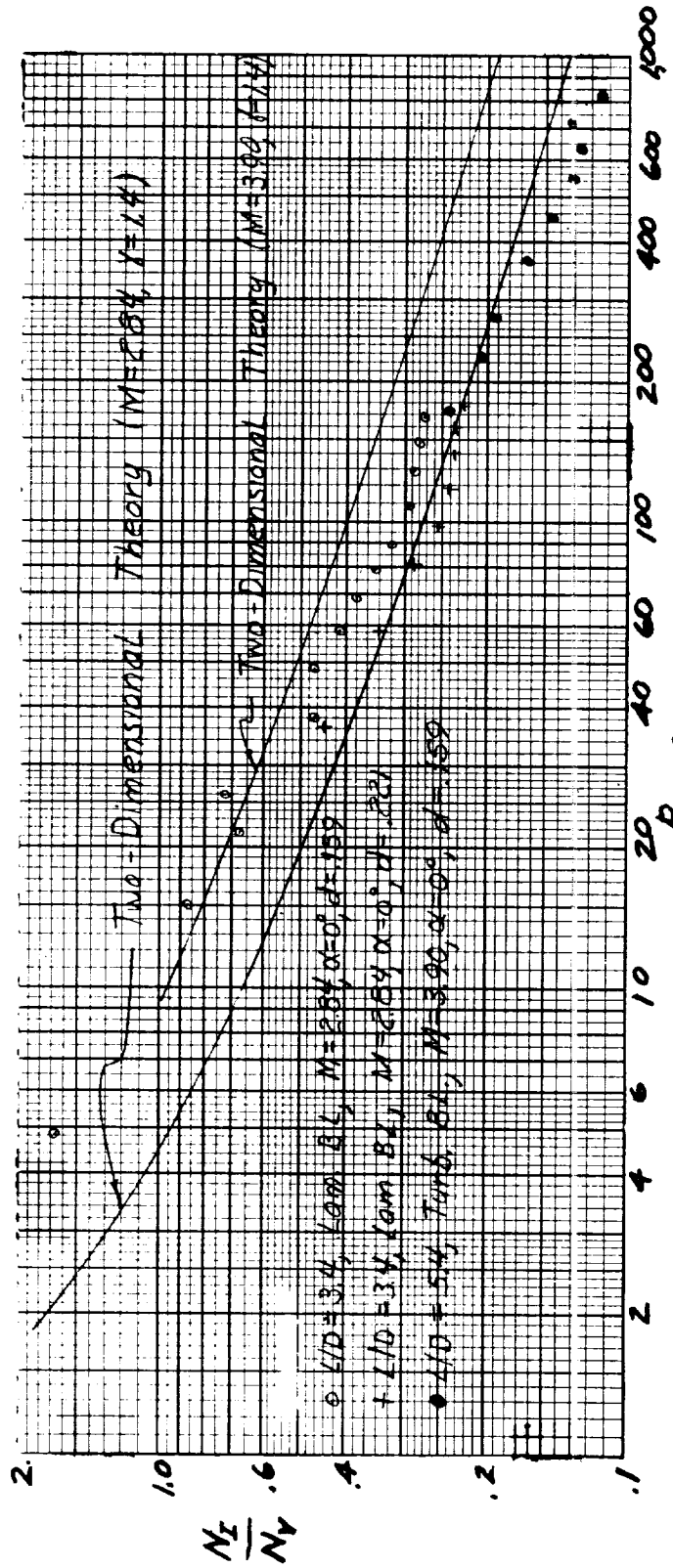

Figure 7.- Comparison of experimental data with two-dimensional theory, $l/D = 0.0625$.

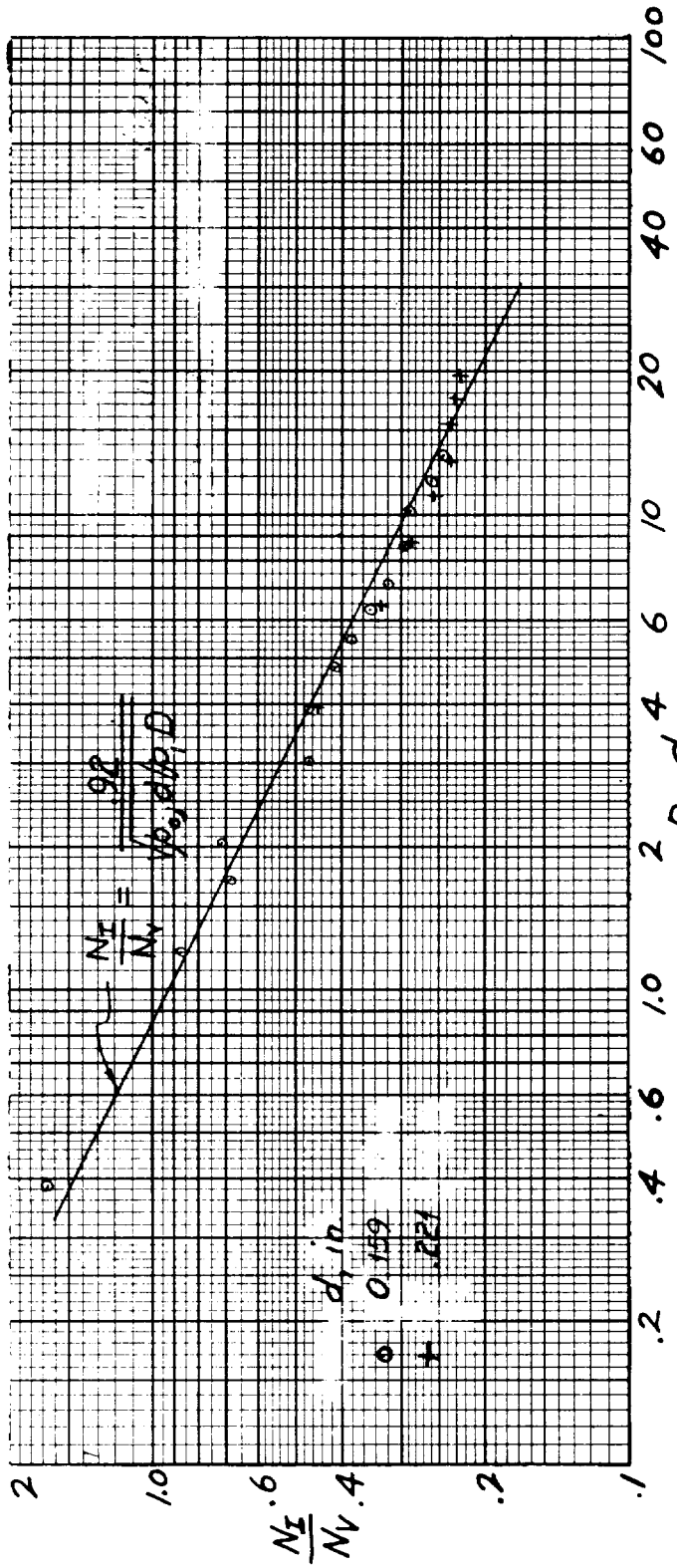

Figure 8.- Effect of jet orifice diameter on interaction force; M = 2.84, $\alpha = 0^{\circ}$, laminar boundary layer, L/D = 3.4, and $l/D = 0.0625$.

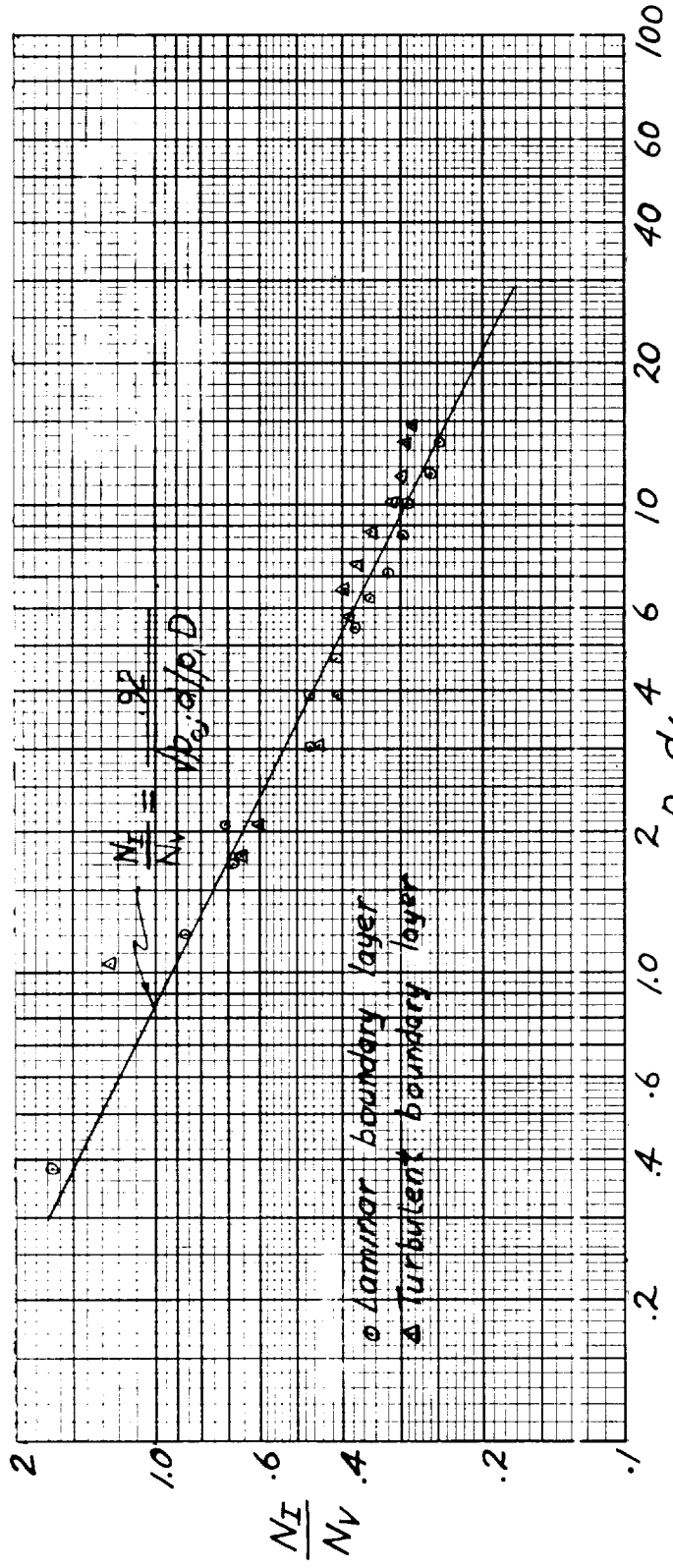

Figure 9.- Effect of boundary-layer condition on interaction force; M = 2.84, $\alpha = 0^{\circ}$, L/D = 3.4, l/D = 0.0625, and d = 0.159 inch.

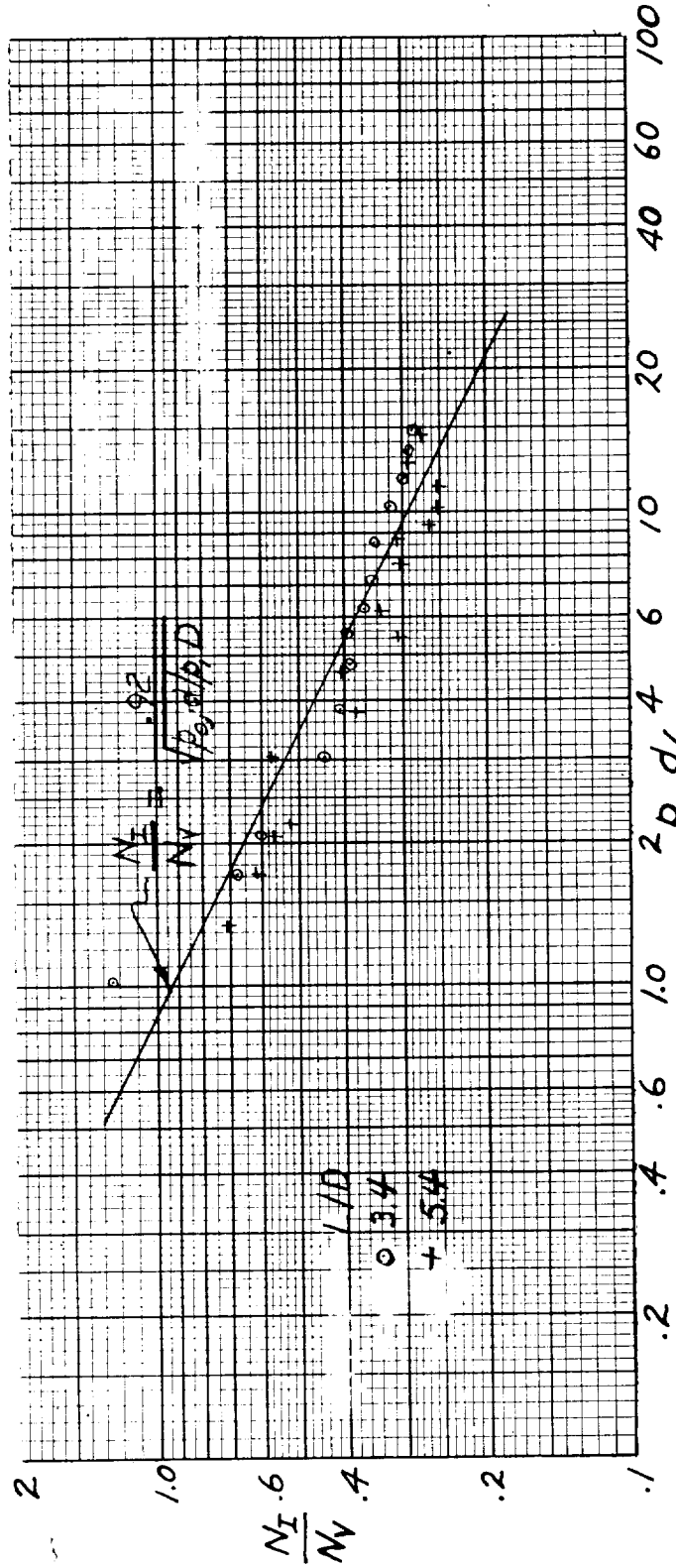

Figure 10.- Effect of forebody length on interaction force; M = 2.84, $\alpha = 0^{\circ}$, turbulent boundary layer, $l/D = 0.0625$, and $d = 0.159$ inch.

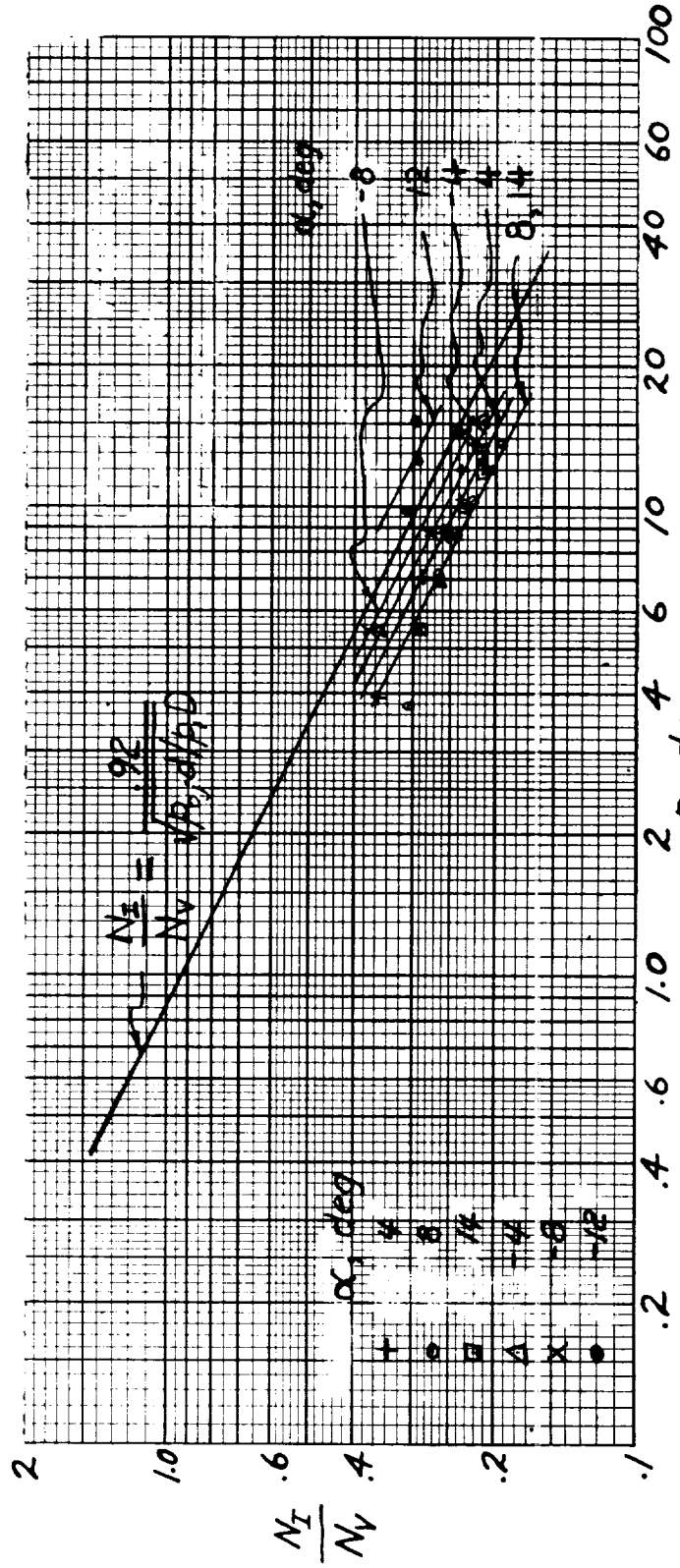

Figure 11.- Effect of angle of attack on interaction force; M = 2.84, L/D = 5.4, turbulent boundary layer, l/D = 0.0625, and d = 0.159 inch.

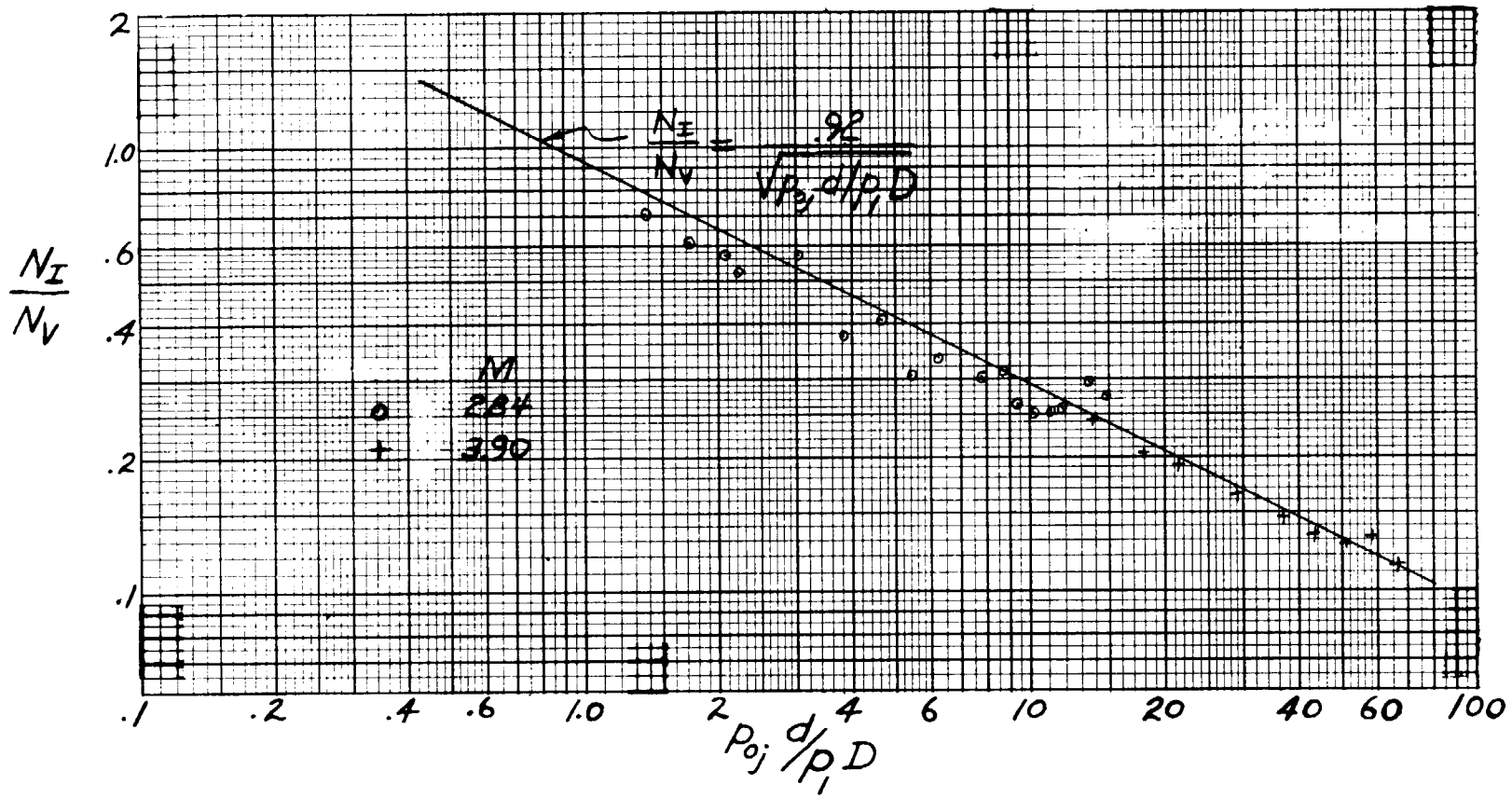

Figure 12.- Effect of Mach number on interaction force; $\alpha = 0^{\circ}$, $L/D = 5.4$, turbulent boundary layer, $l/D = 0.0625$, and $d = 0.159$ inch.

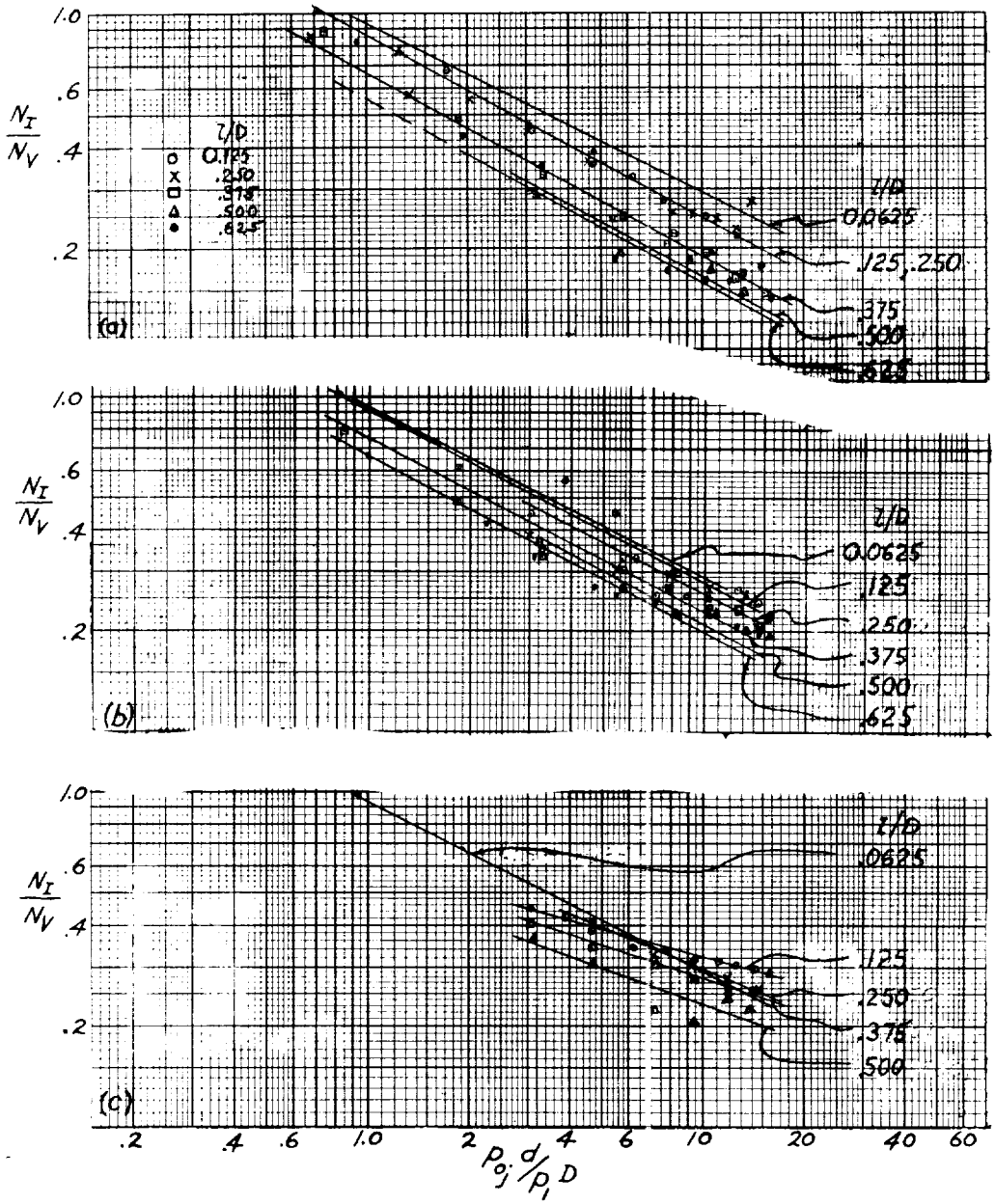

(a) L/D = 3.4, laminar boundary layer.

(b) L/D = 3.4, turbulent boundary layer.

(c) L/D = 5.4, turbulent boundary layer.

Figure 13.- Effect of afterbody length on interaction force; M = 2.84, $\alpha = 0^{\circ}$, and d = 0.159 inch.

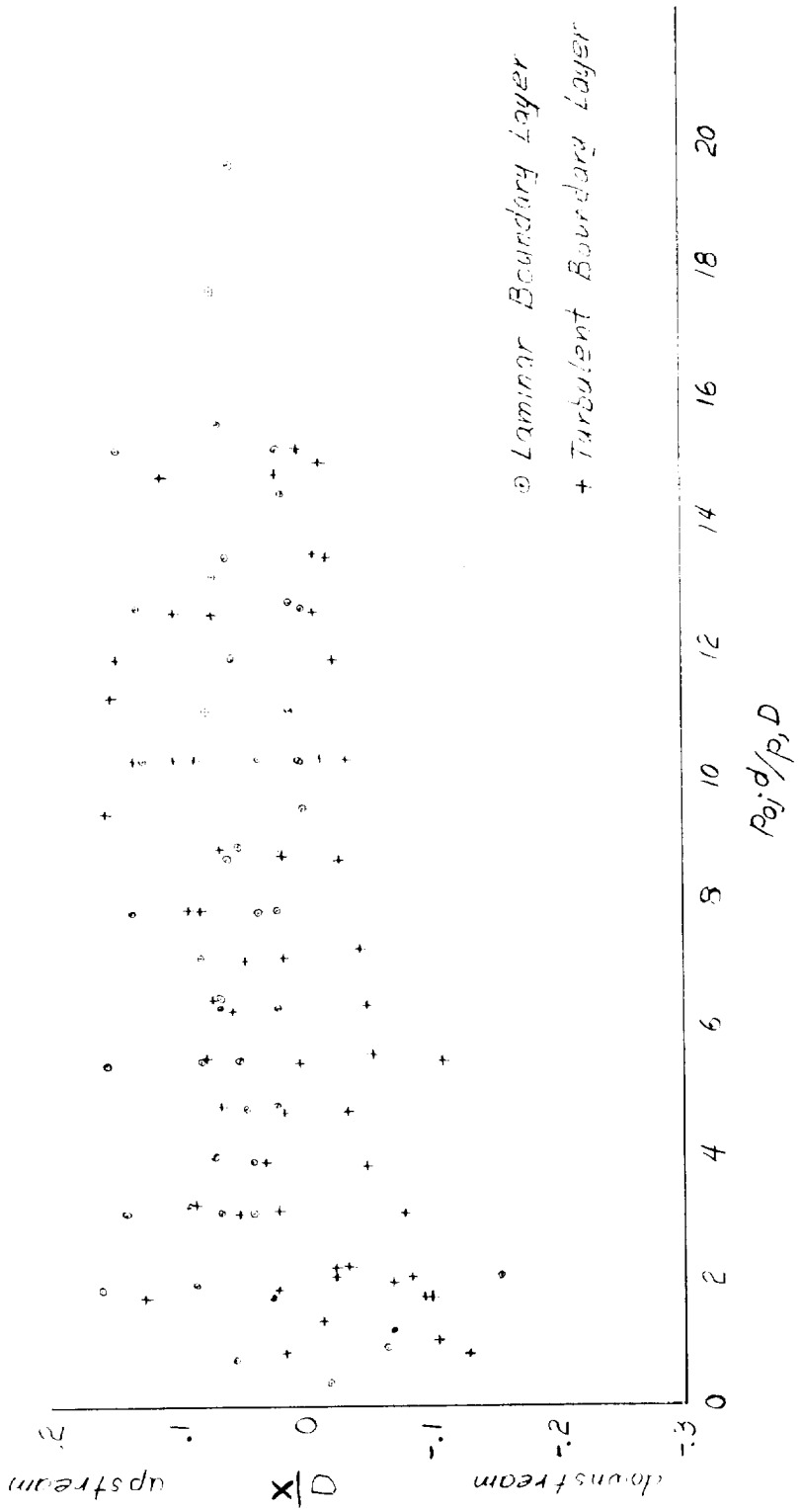

Figure 14.- Location of normal force N_Δ with respect to jet orifice.

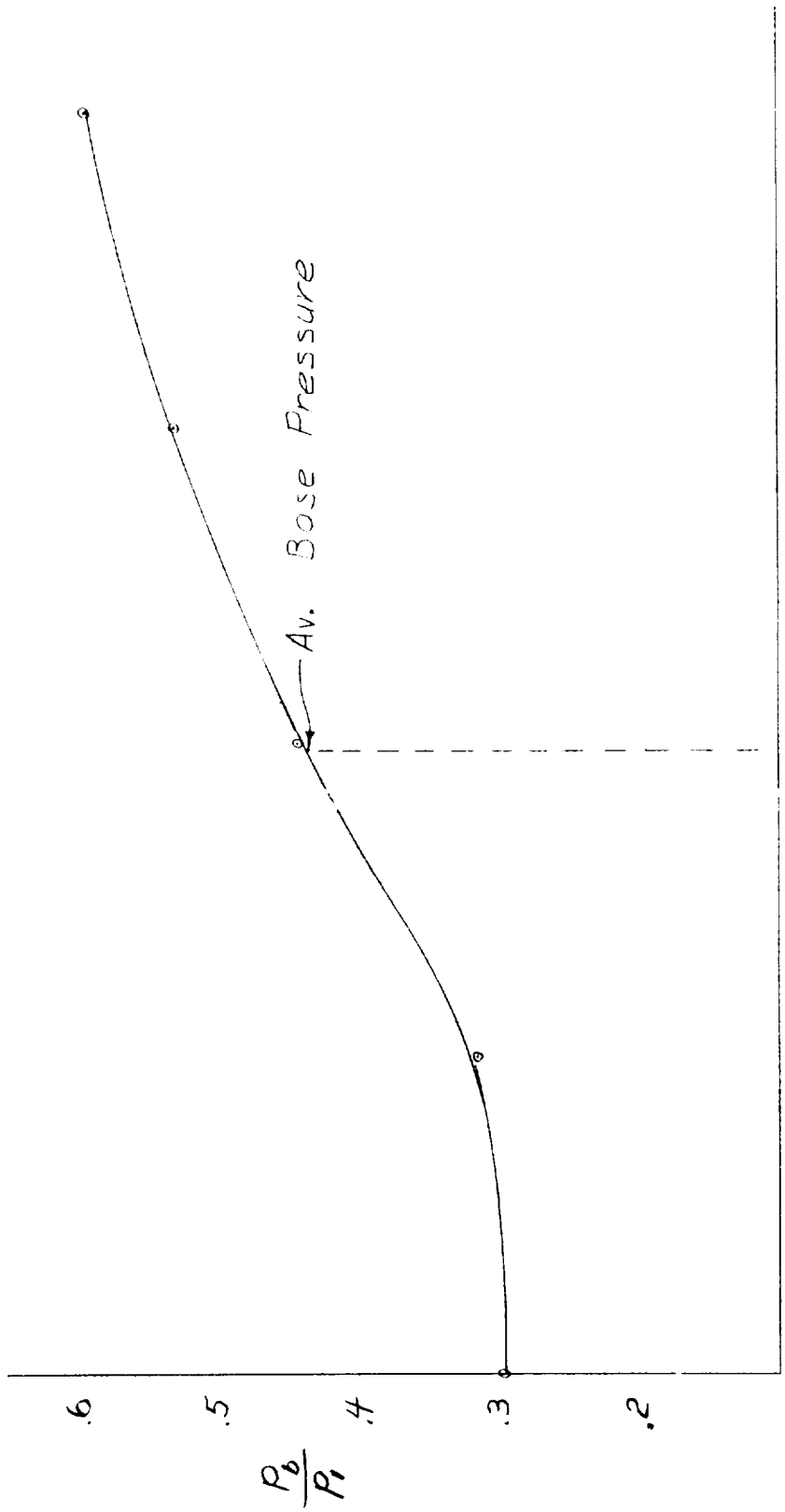

Figure 15.- Circumferential base-pressure variation; M = 2.84, $\alpha = 0^{\circ}$, turbulent boundary layer, L/D = 5.4, l/D = 0.0625, and $p_{0_j} d / p_1 D = 9.4$.

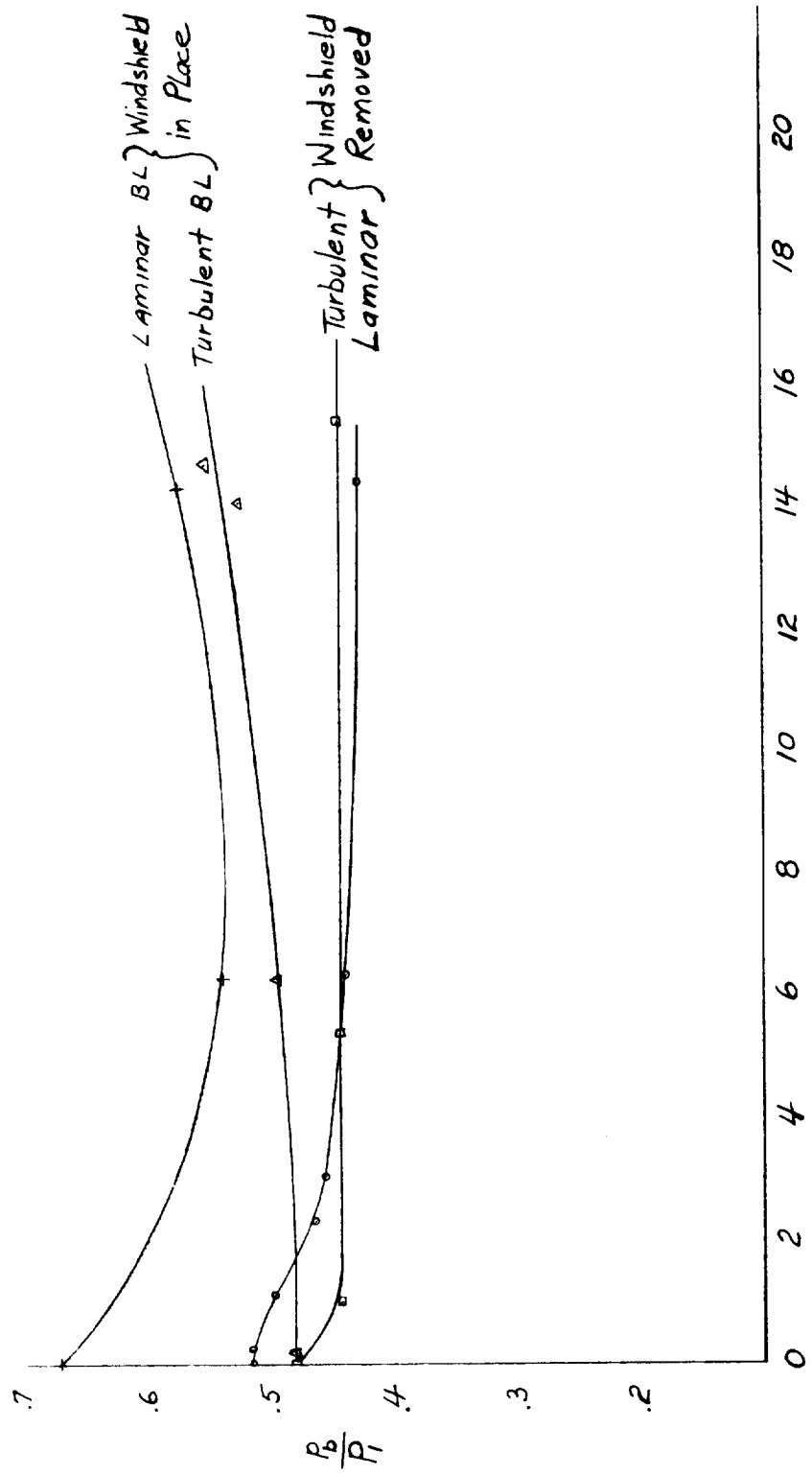

Figure 16.- Effect of side jet on base pressure measured at angular position 90° from jet orifice; L/D = 5.4, M = 2.84, $\alpha = 0^{\circ}$, and $l/D = 0.0625$.

(a) $p_{o_j}/p_1 = 48$, $M = 2.84$.

(b) $p_{o_j}/p_1 = 48$, 90° roll, $M = 2.84$.

(c) $p_{o_j}/p_1 = 69$, $M = 2.84$.

(d) $p_{o_j}/p_1 = 69$, 90° roll, $M = 2.84$.

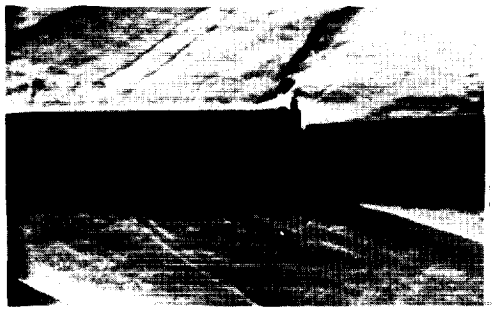

(e) $p_{o_j}/p_1 = 185$, $M = 2.84$.

L-58-3964

(f) $p_{o_j}/p_1 = 188$, 90° roll, $M = 2.84$.

Figure 17.- Turbulent boundary-layer separation ahead of a side jet; $L/D = 5.4$, $l/D = 0.0625$, $\alpha = 0^\circ$, and $d = 0.159$ inch.

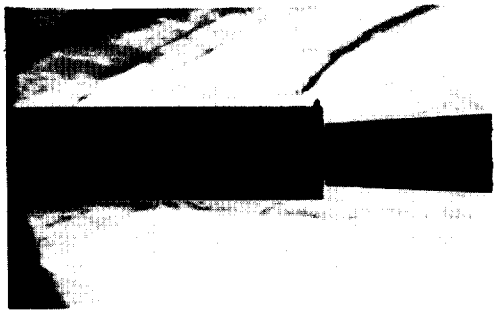

(g) $p_{o_j}/p_1 = 173$, M = 3.90.

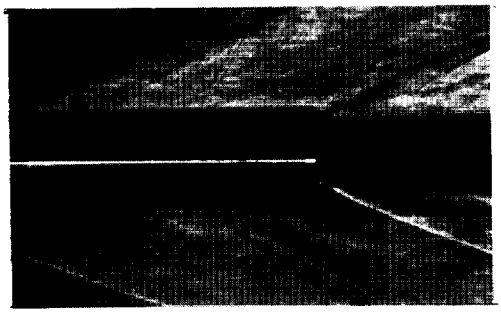

(h) $p_{o_j}/p_1 = 173$, 90° roll, M = 3.90.

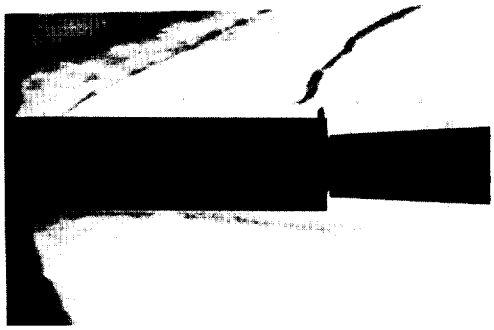

(i) $p_{o_j}/p_1 = 364$, M = 3.90.

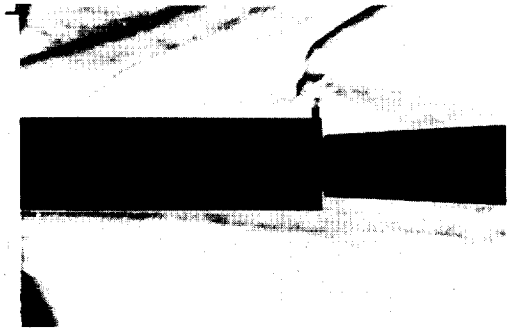

(j) $p_{o_j}/p_1 = 637$, M = 3.90.

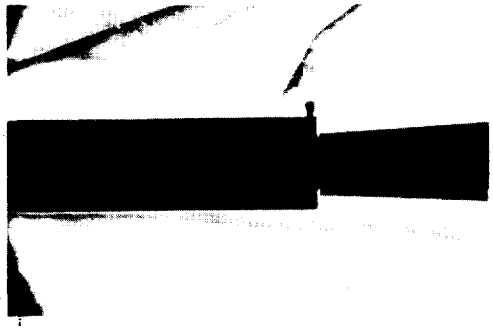

(k) $p_{o_j}/p_1 = 830$, M = 3.90.

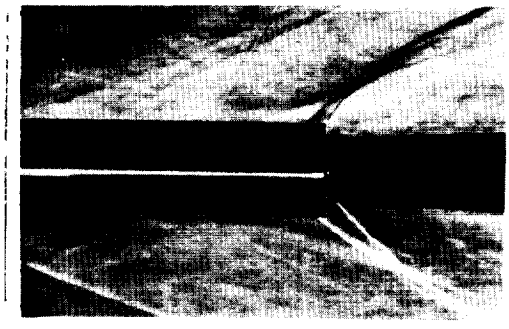

L-58-3965

(l) $p_{o_j}/p_1 = 907$, 90° roll, M = 3.90.

Figure 17.- Concluded.

(a) $p_{o_j}/p_1 = 34$, laminar boundary layer.

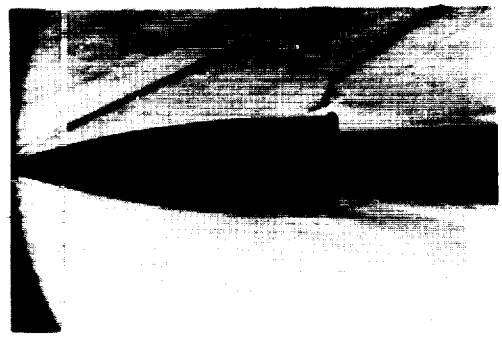

(b) $p_{o_j}/p_1 = 34$, turbulent boundary layer.

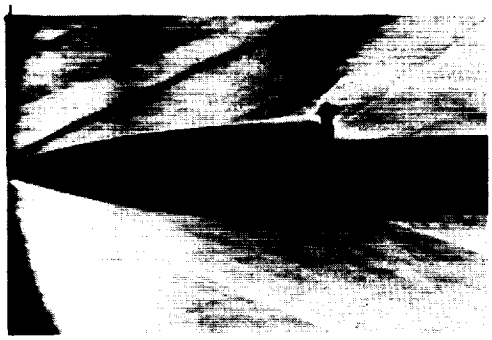

(c) $p_{o_j}/p_1 = 163$, laminar boundary layer.

(d) $p_{o_j}/p_1 = 162$, turbulent boundary layer.

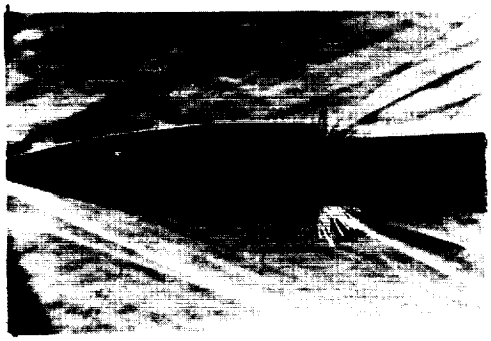

(e) $p_{o_j}/p_1 = 34$, 90° roll, laminar boundary layer.

L-58-3966

(f) $p_{o_j}/p_1 = 161$, 90° roll, laminar boundary layer.

Figure 18.- Laminar and turbulent separation ahead of a side jet; $M = 2.84$, $L/D = 3.4$, $l/D = 0.0625$, $\alpha = 0^\circ$, and $d = 0.221$ inch.

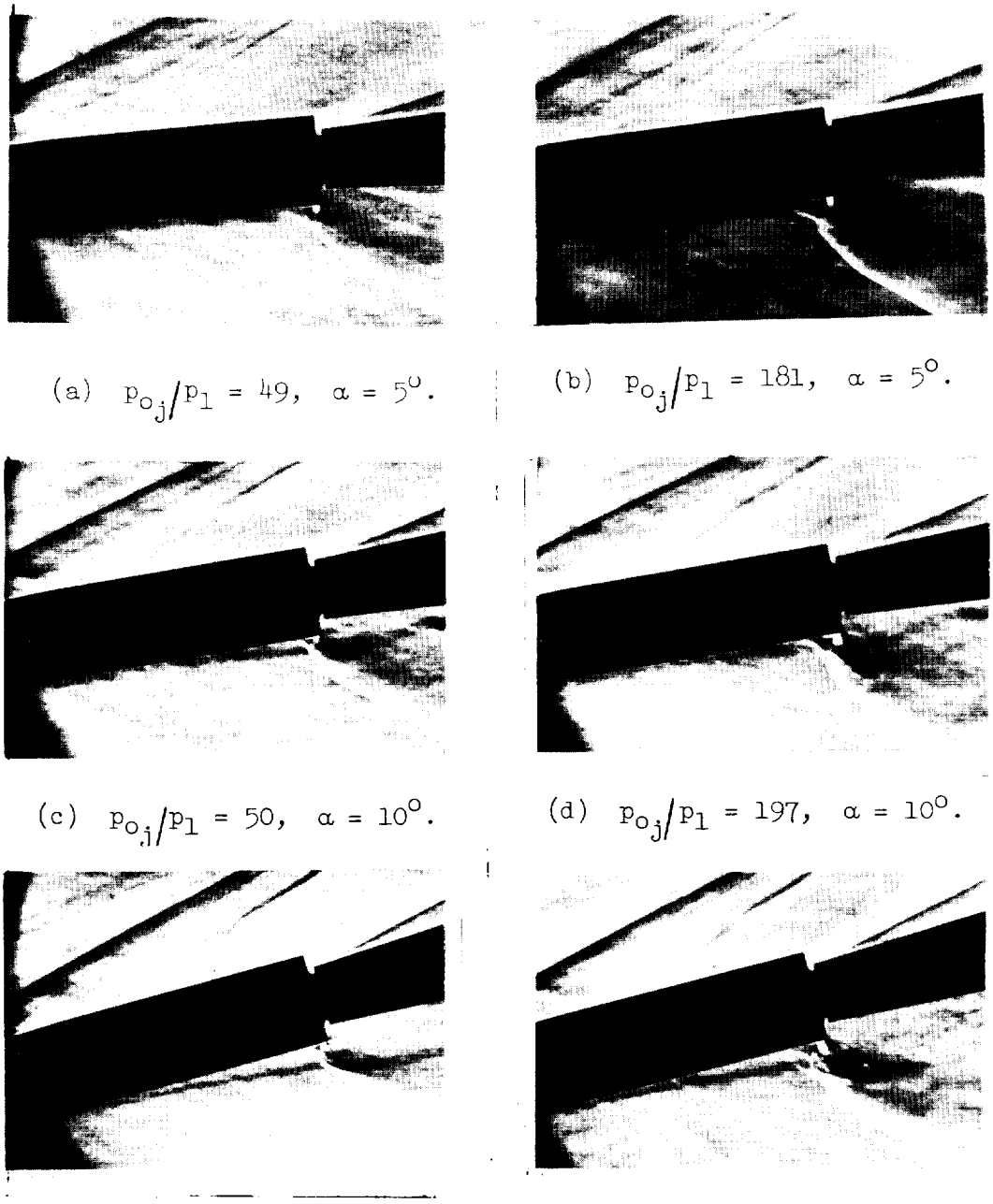

(a) $p_{o_j}/p_1 = 49$, $\alpha = 5^\circ$.

(b) $p_{o_j}/p_1 = 181$, $\alpha = 5^\circ$.

(c) $p_{o_j}/p_1 = 50$, $\alpha = 10^\circ$.

(d) $p_{o_j}/p_1 = 197$, $\alpha = 10^\circ$.

(e) $p_{o_j}/p_1 = 47$, $\alpha = 14^\circ$.

(f) $p_{o_j}/p_1 = 175$, $\alpha = 14^\circ$.

L-58-3967

Figure 19.- Turbulent separation ahead of a side jet at positive and negative angles of attack; M = 2.84, L/D = 5.4, l/D = 0.0625, and d = 0.159 inch.

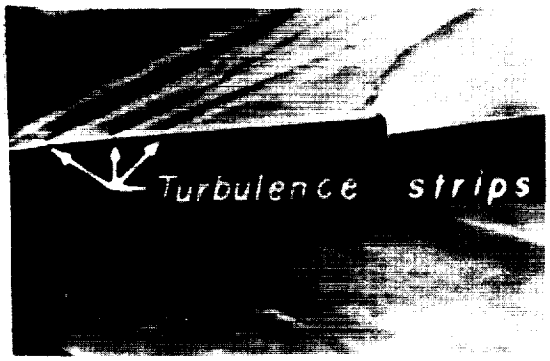

(g) $p_{o_j}/p_1 = 67$, $\alpha = -4^\circ$.

(h) $p_{o_j}/p_1 = 188$, $\alpha = -4^\circ$.

(i) $p_{o_j}/p_1 = 68$, $\alpha = -8^\circ$.

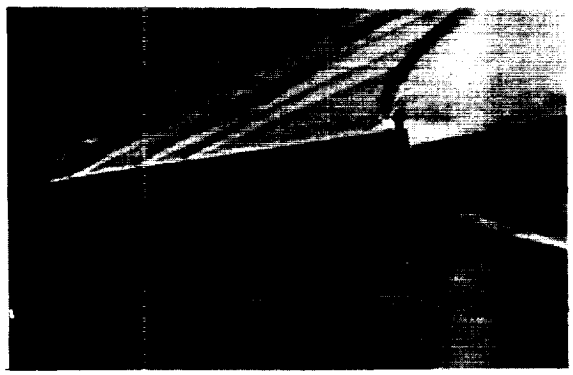

(j) $p_{o_j}/p_1 = 177$, $\alpha = -8^\circ$.

(k) $p_{o_j}/p_1 = 68$, $\alpha = -12^\circ$.

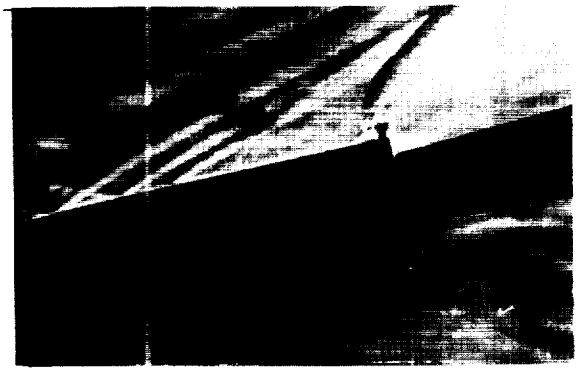

L-58-3968

(l) $p_{o_j}/p_1 = 189$, $\alpha = -12^\circ$.

Figure 19.- Concluded.

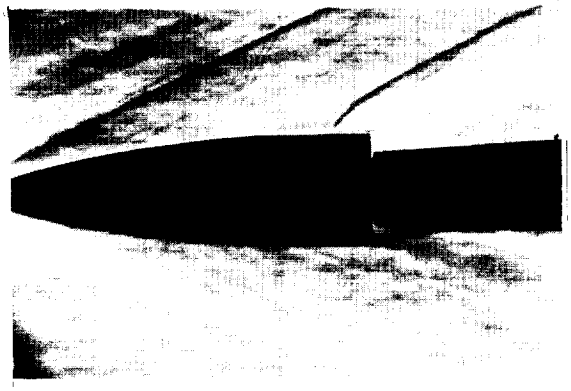

(a) $p_{o_j}/p_1 = 14$, $l/D = 0.25$.

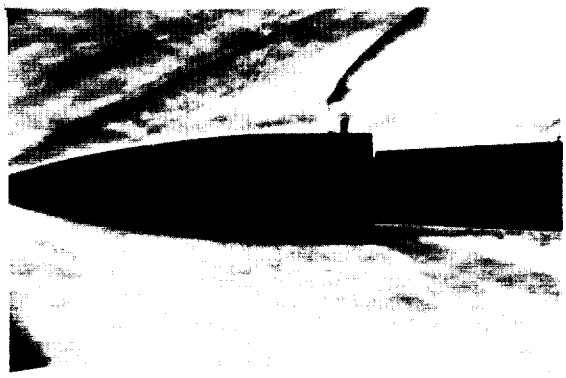

(b) $p_{o_j}/p_1 = 160$, $l/D = 0.25$.

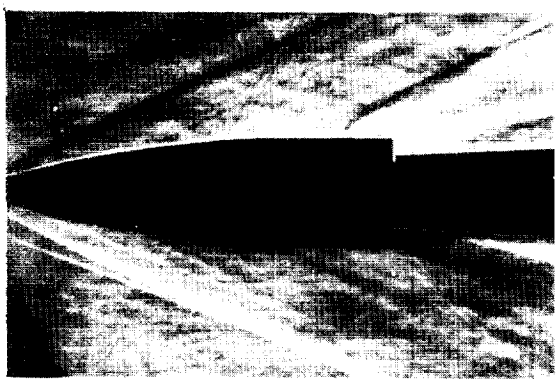

(c) $p_{o_j}/p_1 = 10$, $l/D = 0.375$.

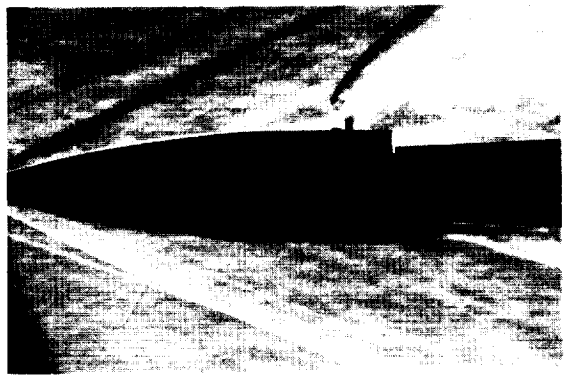

(d) $p_{o_j}/p_1 = 173$, $l/D = 0.375$.

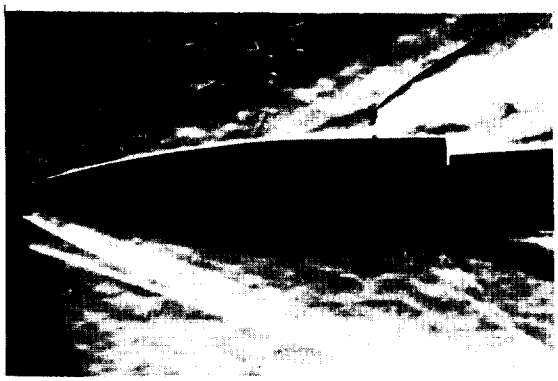

(e) $p_{o_j}/p_1 = 36$, $l/D = 0.625$.

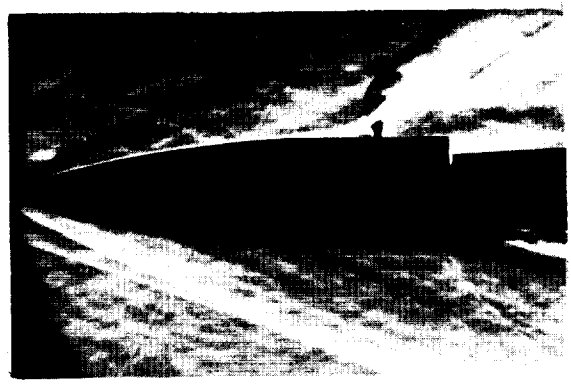

L-58-3969

(f) $p_{o_j}/p_1 = 173$, $l/D = 0.625$.

Figure 20.- Laminar separation ahead of a side jet with various afterbody lengths; M = 2.84, L/D = 3.4, $\alpha = 0^{\circ}$, and d = 0.159 inch.

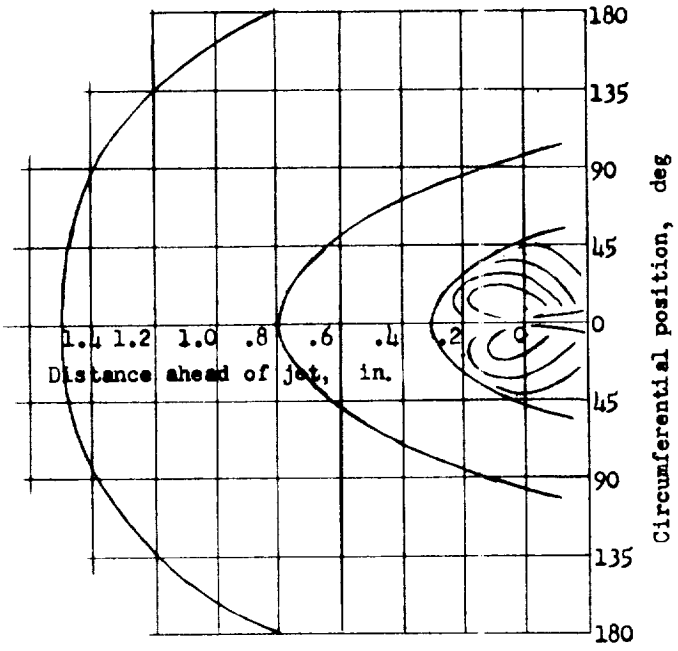

Laminar boundary layer

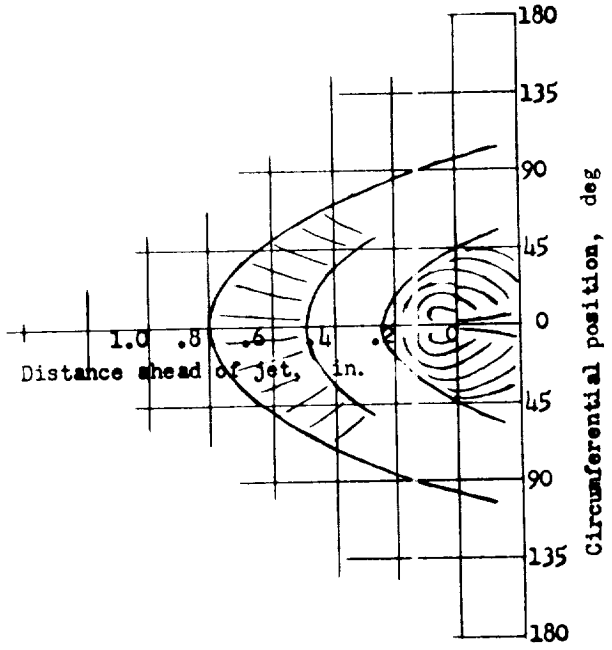

Turbulent boundary layer

Figure 21.- China-clay patterns of flow in vicinity of a side jet; $p_{o_j}/p_1 = 178$, $M = 2.84$, and $\alpha = 0^\circ$.

12-5-58W

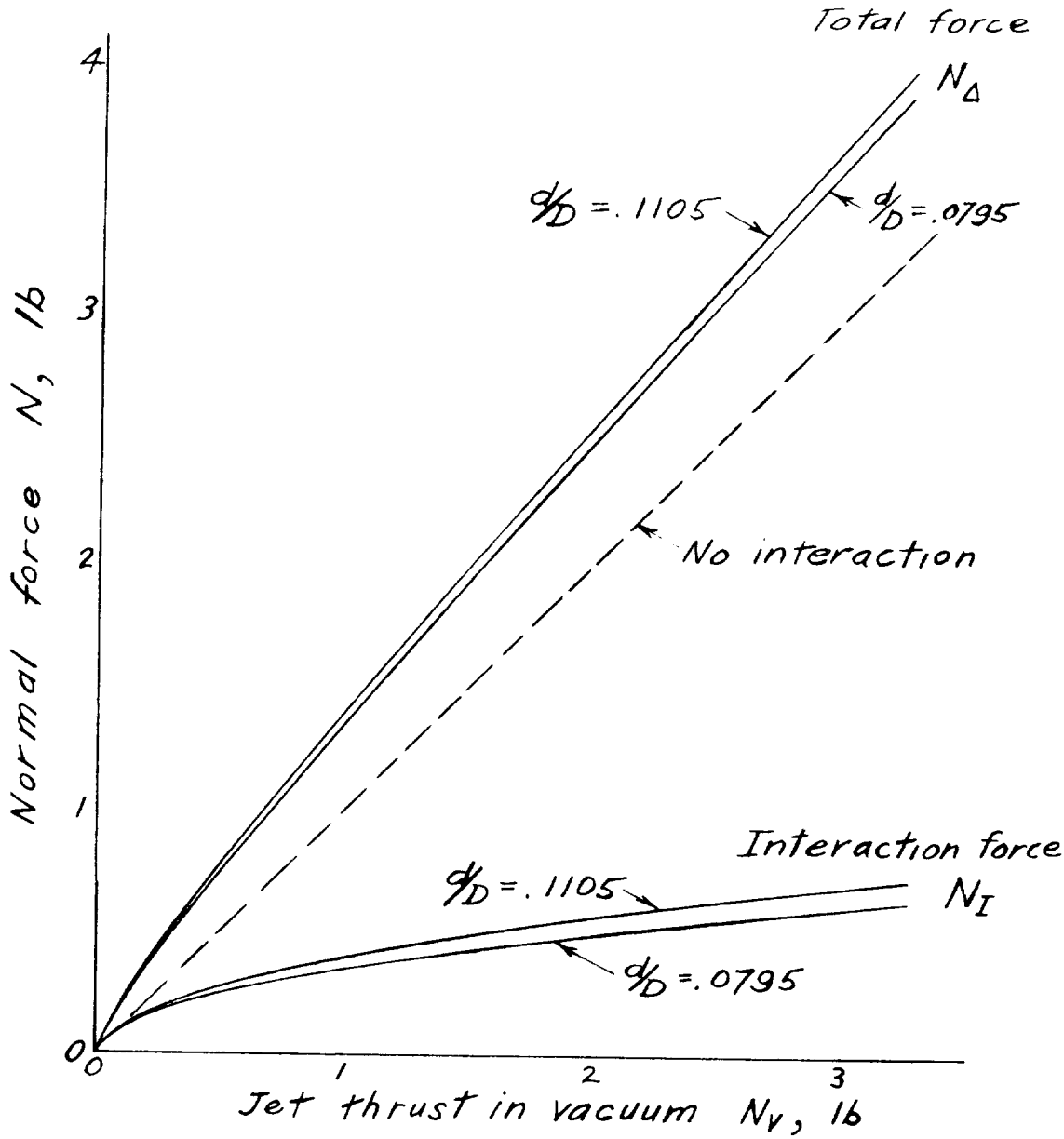

Figure 22.- Variation of normal force with jet thrust; p_1 = 0.5 psia, D = 2 inches.

NASA - Langley Field, Va.